Composite Structures 97 (2013) 147–164

Contents lists available at SciVerse ScienceDirect

Composite Structures

journal homepage: www.elsevier.com/locate/compstruct

Finite deformations of curved laminated St. Venant–Kirchhoff beam using layer-wise third order shear and normal deformable beam theory (TSNDT)

R.C. Batra *, J. Xiao

Department of Engineering Science and Mechanics, M/C 0219, Virginia Polytechnic Institute and State University, Blacksburg, VA 24061, USA

ARTICLE INFO

Article history:
Available online 27 October 2012

Keywords:
TSNDT
Finite deformations
Method of manufactured solutions
St. Venant–Kirchhoff elastic material

ABSTRACT

A layer-wise third order shear and normal deformable plate/shell theory (TSNDT) incorporating all geometric nonlinearities is used to study finite transient deformations of a curved laminated beam composed of a St. Venant–Kirchhoff material. In the TSNDT all displacement components of a point are expressed as 3rd order polynomials in the thickness coordinate in each layer while maintaining the displacement continuity across adjoining layers. No shear correction factor is used. Transverse shear and transverse normal stresses are found from the computed displacement fields and the constitutive relation (i.e., no stress recovery technique is employed). For the St. Venant–Kirchhoff material the strain energy density is a quadratic function of the Green-St. Venant strain tensor appropriate for finite deformations. The software based on the finite element method (FEM) capable of solving static and transient nonlinear problems has been verified by using the method of manufactured solutions. Furthermore, results computed with the TSNDT have been found to agree well with those obtained using the commercial software ABAQUS, and C3D20 elements. Significant contributions of the work include developing a TSNDT considering all geometric nonlinearities and a materially objective constitutive relation, using the method of manufactured solutions to verify the numerical solution of transient nonlinear problems, and showing that results from the plate theory agree well with those from the analysis of plane strain nonlinear problems using the finite elasticity theory. Plate problems using the TSNDT can be analyzed with piecewise linear basis functions in the FEM.

1. Introduction

Laminated composite structures are widely used in aerospace, automobile and marine industries. Numerous plate and shell theories have been developed to analyze deformations of these structures, e.g., see the review articles [1–3]. The classical plate and shell theory (CPT) like the Kirchhoff thin plate theory does not correctly predict results when the plate is moderately thick and shear deformations are not negligible. The first order shear deformable plate theory (FSDT) such as the Reissner–Mindlin theory [4,5] considers transverse shear deformations and gives good results for moderately thick plates but it needs a shear correction factor and the transverse shear and transverse normal stresses are generally computed by using a stress recovery technique. Reddy and Liu [6] proposed a higher-order shear deformable plate theory (HSDT) in which the transverse deflection is independent of the thickness coordinate, z, and the two in-plane displacement components have terms of degree zero, one and three in z. Coefficients of these terms are such that for infinitesimal deformations, the transverse shear strains vanish on the top and the bottom surfaces of the plate; thus boundary-value problems involving tangential loads on these surfaces may not be properly studied.

For laminated plates, in order for the transverse shear and the transverse normal stresses to be continuous across an interface between adjoining layers, the transverse shear and the transverse normal strains should, in general, be discontinuous. As pointed out by Carrerra [1], Lekhnitskii [7] was the first to propose a Zig–Zag theory that satisfied the continuity of the transverse shear and the transverse normal stresses in a layered beam. Assuming a plane state of stress, Lekhnitskii used the Airy stress function to satisfy equilibrium equations in each layer. Strains were derived from stresses by using Hooke's law and strain–displacement equations were integrated for displacements to ensure the continuity of displacements across interfaces between adjoining layers. Ren [8,9] extended Lekhnitskii's theory to orthotropic and anisotropic plates, using this theory Ren and Owen [10] studied vibrations and buckling of beams. Ambartsumian [11] extended the Reissner–Mindlin plate theory to layered anisotropic plates and shells. The assumed displacement field in each layer involved transverse shear stresses in a layer and unknown functions of displacements. Whitney [12] applied and extended Ambartsumian's theory to anisotropic and symmetrical and

* Corresponding author. Tel.: +1 5402316051; fax: +1 5402314574.
E-mail addresses: rbatra@vt.edu (R.C. Batra), xiaojian@vt.edu (J. Xiao).

0263-8223/$ - see front matter © 2012 Elsevier Ltd. All rights reserved.
http://dx.doi.org/10.1016/j.compstruct.2012.09.039

nonsymmetrical plates. Reissner [13] used a mixed variational principle to derive the governing equations. The assumed stress and displacement fields a priori satisfy the continuity of displacements and transverse shear stresses across interfaces between adjoining layers. Carrerra [1] has pointed out Koiter's [14] recommendation (KR) that effects of transverse shear and normal stresses be considered in a plate/shell theory. Rybov [15,16] seems to be the first one to incorporate KR in a plate theory by assuming expressions for transverse displacement and transverse shear stresses. Rassakazov [17] adopted KR in plate and shell theories and analyzed analytically and numerically linear and nonlinear problems. The reader is referred to Carrerra's [1] review paper for a historical development and details of various Zig–Zag theories.

Carrera [18,19] developed the equivalent single layer (ESL) and layer-wise Zig- Zag plate theories based on Reissner's work. Di Sciuva [20] proposed a through-the-thickness piece-wise linearly varying displacement field which satisfies the continuity of surface tractions between adjoining layers and the number of unknowns is independent of the number of layers. Cho and Parmerter [21] generalized Di Sciuva's work by superposing a cubic varying displacement field on a zig–zag varying displacement field. Wu and Chen [22] developed a higher order theory based on global–local superposition technique that can accurately predict transverse shear stresses directly from constitutive relations and displacement fields found using the plate theory.

The transverse normal deformation becomes important when the plate is either thick or differences in values of elastic constants of materials of adjoining layers are large or major surfaces of the plate are subjected to equal and opposite normal tractions or the plate material is soft. A typical sandwich structure is composed of stiff face sheets and a flexible core; thus elastic constants of materials of the core and the face sheets vary significantly. In order to ascertain damage and failure of sandwich structures, it is critical that stresses be accurately found. One way to do so is to adopt the KR and modify higher order plate or shell theories that do not consider the transverse normal deformation and incorporate in them effects of transverse deformations. Batra and Vidoli [23,24] used the Reissner mixed variational principle to derive a Kth order plate theory in which the three displacement components are assumed to be complete polynomials of degree K in the thickness coordinate z. They considered infinitesimal deformations of a piezoelectric material in [23] and also analyzed deformations of a thick beam due to tangential tractions; they studied wave propagation in an orthotropic non-piezoelectric material in [24]. Other higher-order plate theories have been deduced by Carrerra [1] and Demassi [25] to cite a few. Carrerra [26] has reviewed various plate theories for multi-layered anisotropic laminates. Vel and Batra [27–29] used the Eshelby–Stroh formalism to analytically analyze static deformations of laminated composites with each layer made of a linear elastic material. This approach satisfies the KR and the continuity of surface tractions and displacements at interfaces between adjacent plies.

Sandwich structures with a soft core undergo large deformations for which geometric and material nonlinear effects should be considered. Reddy [30], amongst others, studied deformations of laminated composite plates with a layer-wise theory considering von Karman geometric nonlinearity. Dvorkin and Bathe [31] studied large deformations of plates and shells using four-node shell elements, and derived governing equations for incremental displacements with the virtual work principle. Arciniega and Reddy [32] used a first-order shell theory with seven parameters including thickness stretching, nonlinear strain–displacement relations, three-dimensional constitutive relations, and higher-order elements with Lagrange interpolations.

Here we use a materially objective constitutive relation to study finite deformations of a curved laminated beam, and express displacements in each layer by using the TSNDT ensuring that displacements are continuous across the interface between two adjoining layers, consider all nonlinear effects in strain–displacement relations, and assume that each layer is made of a St. Venant–Kirchhoff material. For this material and with the reference configuration stress free, the 2nd Piola–Kirchhoff stress tensor is a linear function of the Green-St. Venant strain tensor and satisfies the principle of material objectivity. We note that the expression for the first Piola–Kirchhoff stress involves terms that are at least cubic in displacement gradients and that for the Cauchy stress is a ratio of polynomials in displacement gradients. The continuity of surface tractions across an interface between two layers is implicitly satisfied by assuming that the total work done by these surface tractions in any virtual displacement is zero. We use the method of manufactured solutions (e.g., see the material just before and after Eq. (20) of [33]) to verify that numerical solutions of nonlinear problems solved herein are accurate. The present zig–zag TSNDT does not exhibit locking effects, incorporates the KR, and transverse shear and transverse normal stresses are computed by using the 3-D constitutive relations and displacement fields found using the plate theory; thus no stress recovery technique is employed.

The rest of the paper is organized as follows: In Section 2, we summarize equations governing finite static and dynamic deformations of a curved beam in orthogonal curvilinear coordinates. The weak form of governing equations is derived in Section 3, and details of the FEM to numerically solve the initial-boundary-value problem are provided. The layer-wise TSNDT displacement field for a laminated beam is briefly summarized in Section 4. The method of manufactured solutions is used in Section 5 to verify the developed software, and results for several example problems are presented and discussed. Conclusions of this work are summarized in Section 6.

2. Problem formulation

2.1. Kinematics

We study finite plane strain deformations of a curved beam of rectangular cross-section; a schematic sketch of the beam is shown in Fig. 1. Let y_1, y_2, y_3 be orthogonal curvilinear coordinate axes in the reference configuration with y_1-axis along the tangent to the mid-surface of the beam, y_2-axis pointing into the plane of the paper, and y_3-axis pointing along the local thickness direction. Let X_1, X_2, X_3 be fixed rectangular Carstesian coordinate axes, and the y_2-axis be parallel to the x_2- and X_2- axes. Let position vectors, with respect to fixed rectangular Cartesian coordinate axes, of a point p located at (y_1,y_2,y_3) in the reference configuration be x and X in the current and the reference configurations, respectively. The displacement $\boldsymbol{u}$ of point p is given by

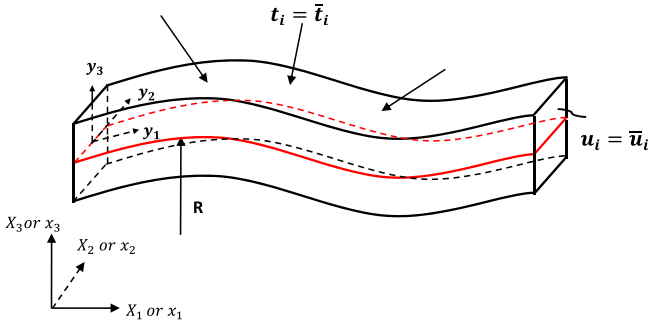

Fig. 1. Schematic sketch of a curved beam.

$$\boldsymbol{u} = \boldsymbol{x} - \boldsymbol{X} \tag{1}$$

where $u_2 = 0$, $u_1 = u_1\,(y_1, y_3, t)$, $u_2 = u_2\,(y_1, y_3, t)$, t is the time.

The components, G_{ij}, of the metric tensor in the reference configuration are given by

$$G_{ij} = \boldsymbol{A}_i \cdot \boldsymbol{A}_j, \quad \boldsymbol{A}_i = \frac{\partial \boldsymbol{X}}{\partial y_i} \tag{2}$$

For orthogonal curvilinear coordinate axes G_{ij} is non-zero only when $i = j$. Let

$$H_1 = \sqrt{G_{11}}, \quad H_2 = \sqrt{G_{22}} = 1, \quad H_3 = \sqrt{G_{33}} = 1,$$
$$\tilde{e}_i = \frac{A_i}{H_{(i)}} \ \text{(no sum on } i\text{)} \tag{3}$$

Here $(\tilde{e}_1, \tilde{e}_2, \tilde{e}_3)$ are unit base vectors for the curvilinear coordinate axes in the reference configuration. We note that

$$H_1 = \left(1 + \frac{y_3}{R}\right), \quad \frac{\partial \tilde{e}_1}{\partial y_1} = -\frac{\tilde{e}_3}{R}, \quad \frac{\partial \tilde{e}_3}{\partial y_1} = \frac{\tilde{e}_1}{R} \tag{4}$$

where R is the radius of curvature at the point (y_1, y_2, y_3).

Following [34], physical components of the displacement gradient, $\boldsymbol{F}$, are given by

$$[F] = \begin{bmatrix} 1 + \frac{1}{H_1}\left(\frac{\partial u_1}{\partial y_1} + \frac{u_3}{R}\right) & 0 & \frac{\partial u_1}{\partial y_3} \\ 0 & 1 & 0 \\ \frac{1}{H_1}\left(\frac{\partial u_3}{\partial y_1} - \frac{u_1}{R}\right) & 0 & 1 + \frac{\partial u_3}{\partial y_3} \end{bmatrix} \tag{5}$$

The Green-St. Venant strain tensor, $\boldsymbol{E}$, defined by

$$\boldsymbol{E} = \frac{1}{2}(\boldsymbol{F}^T\boldsymbol{F} - \boldsymbol{1}) \tag{6}$$

where $\boldsymbol{1}$ is the identity tensor, has the following non-zero physical components:

$$E_{11} = \frac{1}{H_1}\left(\frac{\partial u_1}{\partial y_1} + \frac{u_3}{R}\right) + \frac{1}{2H_1^2}\left[\left(\frac{\partial u_1}{\partial y_1} + \frac{u_3}{R}\right)^2 + \left(\frac{\partial u_3}{\partial y_1} - \frac{u_1}{R}\right)^2\right]$$
$$E_{33} = \frac{\partial u_3}{\partial y_3} + \frac{1}{2}\left[\left(\frac{\partial u_1}{\partial y_3}\right)^2 + \left(\frac{\partial u_3}{\partial y_3}\right)^2\right]$$
$$2E_{13} = \frac{1}{H_1}\left(\frac{\partial u_3}{\partial y_1} - \frac{u_1}{R}\right) + \frac{\partial u_1}{\partial y_3} + \frac{1}{H_1}\left[\frac{\partial u_3}{\partial y_3}\left(\frac{\partial u_3}{\partial y_1} - \frac{u_1}{R}\right) + \frac{\partial u_1}{\partial y_3}\left(\frac{\partial u_1}{\partial y_1} + \frac{u_3}{R}\right)\right] \tag{7}$$

We note that $\boldsymbol{E}$ incorporates all geometric nonlinearities including the von Kármán nonlinearity, and is valid for finite (or large) deformations of a beam. The strain tensor for infinitesimal deformations is obtained from Eq. (7) by neglecting the nonlinear terms included in brackets.

Recalling that beam's dimension along the y_3- (or the z-) axis is considerably smaller than that along the y_1-axis, we assume the following 3rd order Taylor series expansion in y_3 for u_1 and u_3:

$$u_1(y_1, y_3, t) = \sum_{i=0}^{3} (y_3)^i u_{1i}(y_1, t) = L_i(y_3) u_{1i}(y_1, t) \tag{8.a}$$
$$u_3(y_1, y_3, t) = \sum_{i=0}^{3} (y_3)^i u_{3i}(y_1, t) = L_i(y_3) u_{3i}(y_1, t) \tag{8.b}$$
$$L_j(y_3) = (y_3)^j, \quad j = 0, 1, 2, 3 \tag{8.c}$$
$$L_j'(y_3) = \mathrm{D}_{ji} L_i(y_3) \ \text{(summed on } i; i, j = 0, 1, 2, 3) \tag{8.d}$$
$$[\mathrm{D}] = \begin{bmatrix} 0 & 0 & 0 & 0 \\ 1 & 0 & 0 & 0 \\ 0 & 2 & 0 & 0 \\ 0 & 0 & 3 & 0 \end{bmatrix} \tag{8.e}$$

Here and below a repeated index implies summation over the range of the index, and a repeated index enclosed in parentheses does not imply summation. In Eq. (8), u_{10} and u_{30} are, respectively, the axial and the transverse displacements of a point on beam's mid-surface, u_{1i} and $u_{3i} (i = 1, 2, 3)$ may be interpreted as generalized axial and transverse displacements of a point. The first subscript on u corresponds to the displacement direction, and the second subscript to the power of y_3. For $u_{10} = u_{12} = u_{13} = u_{31} = u_{32} = u_{33} = 0$, we get the Euler–Bernoulli beam theory when $u_{11} = -\frac{\partial u_{30}}{\partial y_1}$ and the Timoshenko beam theory when u_{11} is an arbitrary function of y_1 and time t. The displacement field (8) is a special case of the Kth order displacement field considered, amongst others, by Batra and Vidoli [23,24], Carerra [1], Lo et al. [35], and Cho et al. [36]. We call the beam theory based on Eq. (8) as the third-order shear and normal deformable theory (TSNDT). Note that it accounts for the transverse normal strain and does not assume the transverse shear strain at the top and the bottom surfaces to be zero. Substitution for u_1 and u_3 from Eq. (8) into Eqs. (5) and (7) gives the following expressions for physical components of deformation gradient $\boldsymbol{F}$ and non-zero physical components of the Green-St. Venant strain tensor $\boldsymbol{E}$:

$$[F] = \begin{bmatrix} 1 + L_j \frac{1}{H_1}\left(\frac{\partial u_{1j}}{\partial y_1} + \frac{u_{3j}}{R}\right) & 0 & L_j D_{bj} u_{1b} \\ 0 & 1 & 0 \\ L_j \frac{1}{H_1}\left(\frac{\partial u_{3j}}{\partial y_1} - \frac{u_{1j}}{R}\right) & 0 & 1 + L_j D_{bj} u_{3b} \end{bmatrix}$$

$$E_{11} = L_j \frac{1}{H_1}\left(\frac{\partial u_{1j}}{\partial y_1} + \frac{u_{3j}}{R}\right) + \frac{1}{2H_1^2} L_i L_j \times \left(\frac{\partial u_{1i}}{\partial y_1}\frac{\partial u_{1j}}{\partial y_1} + \frac{u_{3i}u_{3j}}{R^2} + 2\frac{u_{3i}}{R}\frac{\partial u_{1j}}{\partial y_1} + \frac{\partial u_{3i}}{\partial y_1}\frac{\partial u_{3j}}{\partial y_1} + \frac{u_{1i}u_{1j}}{R^2} - 2\frac{u_{1i}}{R}\frac{\partial u_{3j}}{\partial y_1}\right)$$

$$E_{33} = L_j D_{bj} u_{3b} + \frac{1}{2} L_i L_j (D_{bi} u_{1b} D_{lj} u_{1l} + D_{bi} u_{3b} D_{lj} u_{3l}) \tag{9}$$

$$2E_{13} = L_j \frac{1}{H_1}\left(\frac{\partial u_{3j}}{\partial y_1} - \frac{u_{1j}}{R}\right) + L_j D_{bj} u_{1b} + \frac{1}{2H_1} L_i L_j \left[D_{bi} u_{3b}\left(\frac{\partial u_{3j}}{\partial y_1} - \frac{u_{1j}}{R}\right) + D_{bi} u_{1b}\left(\frac{\partial u_{1j}}{\partial y_1} + \frac{u_{3j}}{R}\right)\right]$$

where indices $i, j, b, d, l = 0, 1, 2, 3$, and summation on repeated indices is implied. We note that expressions for E_{11}, E_{33} and E_{13} have terms of order 6, 4 and 5, respectively, in y_3. Eq. (9) can be written in the index notation as follows:

$$F_{ma} = \delta_{ma} + \frac{1}{H_{(a)}} L_b e^b_{ma} \tag{10.a}$$
$$E_{\alpha\beta} = \frac{1}{2}\left[L_b\left(\frac{1}{H_{(\beta)}} e^b_{\alpha\beta} + \frac{1}{H_{(\alpha)}} e^b_{\beta\alpha}\right) + L_b L_d \frac{1}{H_{(\alpha)} H_{(\beta)}} \eta^{bd}_{\alpha\beta}\right] \tag{10.b}$$
$$\eta^{bd}_{\alpha\beta} = e^b_{i\alpha} e^d_{i\beta} \tag{10.c}$$

Here indices $b, d = 0,1,2,3$ and the other indices take values 1 and 3, δ_{ma} is the Kronecker delta, and the repeated index enclosed in parentheses is not summed. The non-zero components of $e^j_{\alpha\beta}$ are listed below.

$$e^j_{11} = \frac{\partial u_{1j}}{\partial y_1} + \frac{u_{3j}}{R}, \quad e^j_{13} = D_{bj} u_{1b}, \quad e^j_{31} = \frac{\partial u_{3j}}{\partial y_1} - \frac{u_{1j}}{R},$$
$$e^j_{33} = D_{bj} u_{3b}; \quad j,\ b = 0, 1, 2, 3 \tag{11}$$

2.2. Kinetics

The in-plane displacements (u_1, u_3) of a point are governed by the following equations expressing the balance of linear momentum written in the Lagrangian description of motion using physical

components T_{11}, T_{13}, T_{31}, T_{33}, of the first Piola–Kirchhoff stress tensor [34], and initial and boundary conditions.

$$\rho_0\ddot{u}_1 = \frac{1}{H_1}\frac{\partial T_{11}}{\partial y_1} + \frac{1}{H_1}\frac{\partial (H_1 T_{13})}{\partial y_3} + \frac{1}{H_1 R}T_{31} + f_1 \tag{12.a}$$

$$\rho_0\ddot{u}_3 = \frac{1}{H_1}\frac{\partial T_{31}}{\partial y_1} + \frac{1}{H_1}\frac{\partial (H_1 T_{33})}{\partial y_3} - \frac{1}{H_1 R}T_{11} + f_3 \tag{12.b}$$

$$u_i(y_1, y_3, 0) = u_i^0(y_1, y_3) \tag{12.c}$$

$$\dot{u}_i(y_1, y_3, 0) = \dot{u}_i^0(y_1, y_3) \tag{12.d}$$

$$T_{ij}N_j = \bar{t}_i(y_1, y_3, t) \text{ on } \Gamma_t \tag{12.e}$$

$$u_i(y_1, y_3, t) = \bar{u}_i(y_1, y_3, t) \text{ on } \Gamma_u \tag{12.f}$$

Here i and j equal 1 and 3. In Eq. (12) f_1 and f_3 are components of the body force per unit reference volume along the y_1- and the y_3- axes, respectively, ρ_0 is the mass density in the reference configuration, and $\ddot{u}_i = \frac{\partial^2 u_i}{\partial t^2}$. The initial displacement u_i^0 and the initial velocity $\dot{u}_i^0$ are known functions of y_1 and y_3. Furthermore, $\boldsymbol{N}$ is a unit outward normal in the reference configuration at a point on the boundary Γ_t where surface tractions are prescribed as $\bar{t}_i$. On the remaining boundary, Γ_u, displacements are prescribed as $\bar{u}_i$.

Let $\omega_\alpha(y_1,y_3)(\alpha = 1, 3)$ be smooth functions that vanish on Γ_u. We multiply both sides of Eqs. (12.a) and (12.b) with ω_1 and ω_3, respectively, and integrate the resulting equations over the domain to obtain the following.

$$\int_0^{\mathcal{L}}\int_{-H/2}^{H/2}\omega_1\rho_0\ddot{u}_1 H_1 dy_3 dy_1 = \int_0^{\mathcal{L}}\int_{-H/2}^{H/2}\omega_1 \times\left[\frac{\partial T_{11}}{\partial y_1} + \frac{\partial (H_1 T_{13})}{\partial y_3} + \frac{1}{R}T_{31} + H_1 f_1\right] dy_3 dy_1$$

$$\int_0^{\mathcal{L}}\int_{-H/2}^{H/2}\omega_3\rho_0\ddot{u}_3 H_1 dy_3 dy_1 = \int_0^{\mathcal{L}}\int_{-H/2}^{H/2}\omega_3 \times\left[\frac{\partial T_{31}}{\partial y_1} + \frac{\partial (H_1 T_{33})}{\partial y_3} - \frac{1}{R}T_{11} + H_1 f_3\right] dy_3 dy_1 \tag{13}$$

In Eq. (13), H and $\mathcal{L}$ are the thickness and the length of the beam, respectively. Recalling that functions ω_1, ω_3, u_1 and u_3 do not depend upon y_2, the integration with respect to y_2 has been carried out in Eq. (13) and the common factor (i.e., the width) has been canceled out.

As for $u_\alpha(y_1,y_3)$ in Eq. (8), we write $\omega_\alpha(y_1,y_3)$ as

$$\omega_\alpha(y_1, y_3) = L_j(y_3)\omega_\alpha^j(y_1), \qquad \alpha = 1, 3, \quad j = 0, 1, 2, 3 \tag{14}$$

Substituting from Eq. (14) into Eq. (13) and integrating with respect to y_3, we get

$$\int_0^{\mathcal{L}}\omega_1^j(A_{ji}\ddot{u}_{1i})dy_1 = \int_0^{\mathcal{L}}\omega_1^j\left(\frac{\partial M_{11}^j}{\partial y_1} - D_{ji}M_{13}^i + \frac{1}{R}M_{31}^j + \bar{f}_1^j + B_{13}^j\right)dy_1$$

$$\int_0^{\mathcal{L}}\omega_3^j(A_{ji}\ddot{u}_{3i})dy_1 = \int_0^{\mathcal{L}}\omega_3^j\left(\frac{\partial M_{31}^j}{\partial y_1} - D_{ji}M_{33}^i - \frac{1}{R}M_{11}^j + \bar{f}_3^j + B_{33}^j\right)dy_1 \tag{15}$$

where

$$M_{mn}^j(y_1, t) = \int_{-H/2}^{H/2} L_j(y_3)T_{mn}\mathcal{H}_{(n)}dy_3, \quad \mathcal{H}_{(1)} = 1, \quad \mathcal{H}_{(3)} = H_1 \tag{16.a}$$

$$B_{13}^j(y_1, t) = L_j(H/2)H_1 T_{13}(H/2, t) - L_j(-H/2)H_1 T_{13}(-H/2, t) \tag{16.b}$$

$$B_{33}^j(y_1, t) = L_j(H/2)H_1 T_{33}(H/2, t) - L_j(-H/2)H_1 T_{33}(-H/2, t) \tag{16.c}$$

$$\bar{f}_\alpha^j(y_1, t) = \int_{-H/2}^{H/2} L_j(y_3)f_\alpha H_1 dy_3 \tag{16.d}$$

$$A_{ji}(y_1, t) = \int_{-H/2}^{H/2} L_j(y_3)L_i(y_3)\rho_0 H_1 dy_3 \tag{16.e}$$

and indices m, n, $\alpha = 1, 3$, and $i, j = 0, 1, 2, 3$. The quantity M_{mn}^j equals jth order moment of the stress T_{mn} about the y_2-axis; M_{mn}^0 is usually called the resultant force, and M_{mn}^1 the bending moment. The quantities B_{13}^j and B_{33}^j equal jth order moments about the y_2-axis of the tangential surface traction T_{13} and the normal surface traction T_{33} applied on the top and the bottom surfaces of the beam; for $j = 0$ these equal the resultant forces and for $j = 1$ their first-order moments about the y_2-axis. Similarly, $\bar{f}_\alpha^j$ equals jth order moment of the body force f_α about the y_2-axis, and A_{ji} the inertia tensor associated with the generalized displacements u_{1i} and u_{3i}.

Requiring Eq. (15) to hold for all choices of ω_α^j, we obtain following eight equations governing transient deformations of the beam.

$$A_{ji}\ddot{u}_{1i} = \frac{\partial M_{11}^j}{\partial y_1} - D_{ji}M_{13}^i + \frac{1}{R}M_{31}^j + \bar{f}_1^j + B_{13}^j, \qquad j,\ i = 0, 1, 2, 3 \tag{17.a}$$

$$A_{ji}\ddot{u}_{3i} = \frac{\partial M_{31}^j}{\partial y_1} - D_{ji}M_{33}^i - \frac{1}{R}M_{11}^j + \bar{f}_3^j + B_{33}^j, \qquad j,\ i = 0, 1, 2, 3 \tag{17.b}$$

After expressions for moments M_{mn}^j in terms of displacements have been substituted in Eq. (17), we obtain "governing equations of motion" for the present shell theory which are nonlinear coupled partial differential equations (PDEs) for u_{1j} and u_{3j}. These PDEs involve second-order derivatives of u_{1j} and u_{3j} with respect to y_1 and time t and are to be solved under pertinent initial and boundary conditions.

The traction boundary conditions in Eq. (12.e) on the major surfaces (i.e., the top and the bottom) of the beam have been incorporated in Eq. (17); e.g., see Eqs. (16.b) and (16.c). At the beam edges, $y_1 = 0, y_1 = \mathcal{L}$, we specify a suitable combination of u_{1j}, u_{3j} and $M_{\alpha 1}^j$ given by

$$\int_{-H/2}^{H/2} L_j T_{\alpha 1}dy_3 = M_{\alpha 1}^j, \qquad \alpha = 1, 3; \quad j = 0, 1, 2, 3 \tag{18}$$

We substitute from Eq. (8) into Eqs. (12.c) and (12.d), multiply both sides of the resulting equations with $\rho_0 L_j(y_3)$, and integrate with respect to y_3 on the domain $(-H/2,H/2)$ to obtain the following equations from which initial values $u_{\alpha i}$ $(y_1,0)$ and $\dot{u}_{\alpha i}(y_1, 0)$ are determined.

$$A_{ji}u_{\alpha i}(y_1, 0) = \int_{-H/2}^{H/2}\rho_0 L_j(y_3)u_\alpha^0(y_1, y_3)dy_3 = \mathcal{F}_{\alpha j}(y_1) \tag{19.a}$$

$$A_{ji}\dot{u}_{\alpha i}(y_1, 0) = \int_{-H/2}^{H/2}\rho_0 L_j(y_3)\dot{u}_\alpha^0(y_1, y_3)dy_3 = \dot{\mathcal{F}}_{\alpha j}(y_1) \tag{19.b}$$

Here $\alpha = 1,3$ and $i, j = 0, 1, 2, 3$.

2.3. Constitutive relation

We assume that the beam material is St. Venant–Kirchhoff for which the strain energy density, W, per unit reference volume is given by

$$W = \frac{1}{2}E_{mn}C_{mn\alpha\beta}E_{\alpha\beta}, \quad C_{mn\alpha\beta} = C_{\alpha\beta mn} = C_{nm\alpha\beta} \tag{20}$$

Here $\boldsymbol{C}$ is the fourth-order elasticity tensor having 21 independent components for a general anisotropic material. The independent components of $\boldsymbol{C}$ reduce to 9, 5 and 2 for an orthotropic, transversely isotropic and isotropic material, respectively. The strain energy density for the St. Venant–Kirchhoff material reduces to that of a Hookean material if the finite strain tensor $\boldsymbol{E}$ is replaced in Eq. (20) by the strain tensor $e_{\alpha\beta}^j$ for infinitesimal deformations. Batra [37] has compared the response of four elastic materials for which a stress tensor is a linear function of an appropriate finite strain tensor (e.g., the Cauchy stress tensor is a linear function of the Almansi–Hamel strain tensor). For infinitesimal deformations the four constitutive relations give the same stress–strain curve, but their predictions for finite deformations are quite different.

For a nonlinear elastic material, physical components of the second Piola–Kirchhoff stress tensor $\boldsymbol{S}$ are related to those of $\boldsymbol{E}$ by

$$S_{mn} = \frac{\partial W}{\partial E_{mn}} \tag{21}$$

Eqs. (20) and (21) give

$$S_{mn} = C_{mn\alpha\beta}E_{\alpha\beta} \tag{22}$$

For plane strain deformations of an orthotropic material with the material principal axes coincident with the coordinate axes (y_1,y_2,y_3), Eq. (22) reduces to

$$\begin{Bmatrix} S_{11} \\ S_{33} \\ S_{13} \end{Bmatrix} = \begin{bmatrix} C_{1111} & C_{1133} & 0 \\ C_{3311} & C_{3333} & 0 \\ 0 & 0 & C_{1313} \end{bmatrix} \begin{Bmatrix} E_{11} \\ E_{33} \\ 2E_{13} \end{Bmatrix} \tag{23}$$

Recalling that

$$\boldsymbol{T} = \boldsymbol{FS} \tag{24}$$

where $\boldsymbol{T}$ is the 1st Piola–Kirchhoff stress tensor, we get

$$\begin{bmatrix} T_{11} & T_{13} \\ T_{31} & T_{33} \end{bmatrix} = \begin{bmatrix} F_{11}S_{11} + F_{13}S_{13} & F_{11}S_{13} + F_{13}S_{33} \\ F_{31}S_{11} + F_{33}S_{13} & F_{31}S_{13} + F_{33}S_{33} \end{bmatrix} \tag{25}$$

Substitution for $\boldsymbol{F}$ from Eq. (10.a) into Eq. (25), and for $\boldsymbol{E}$ from Eq. (10.b) into Eq. (23) and the result into Eq. (25) gives expressions for $\boldsymbol{T}$ in terms of generalized displacements u_{1i} and u_{3i} and four elastic constants C_{1111}, C_{1133}, C_{3333}, and C_{1313}. It can be written as

$$\begin{aligned} T_{mn} = {} & \frac{1}{2}\left(\delta_{ma} + \frac{1}{H_{(a)}}L_i e^i_{ma}\right)C_{an\alpha\beta} \\ & \times \left[L_b\left(\frac{1}{H_{(\beta)}}e^b_{\alpha\beta} + \frac{1}{H_{(\alpha)}}e^b_{\beta\alpha}\right) + L_bL_d\frac{1}{H_{(\alpha)}H_{(\beta)}}\eta^{bd}_{\alpha\beta}\right] \end{aligned} \tag{26}$$

Here, indices i, b, d = 0, 1, 2, 3 and other indices take values 1 and 3. Even though components of $\boldsymbol{S}$ are quadratic in displacement gradients those of $\boldsymbol{T}$ are cubic in displacement gradients. Thus constitutive relation (24) accounts for material nonlinearities in the sense that components of $\boldsymbol{T}$ are nonlinear functions of displacement gradients. We note that constitutive relations (21) and (24) are materially objective and are invariant under a rigid body motion superimposed upon the present configuration.

Substituting from Eq. (26) into Eq. (16.a), we obtain

$$\begin{aligned} M^j_{mn} = {} & \int_{-H/2}^{H/2} L_j(y_3)T_{mn}\mathcal{H}_{(n)}dy_3 = \frac{1}{2}\Big[C^{1jb}_{an\alpha\beta}\delta_{ma}e^b_{\alpha\beta} + C^{2jb}_{an\alpha\beta}\delta_{ma}e^b_{\beta\alpha} \\ & + C^{3jbd}_{an\alpha\beta}\delta_{ma}\eta^{bd}_{\alpha\beta} + C^{4jib}_{an\alpha\beta}e^i_{ma}e^b_{\alpha\beta} + C^{5jib}_{an\alpha\beta}e^i_{ma}e^b_{\beta\alpha} + C^{6jibd}_{an\alpha\beta}e^i_{ma}\eta^{bd}_{\alpha\beta}\Big] \end{aligned} \tag{27}$$

where

$$\begin{aligned} & C^{1jb}_{an\alpha\beta} = \int_{-H/2}^{H/2} L_jL_bC_{an\alpha\beta}\frac{\mathcal{H}_{(n)}}{H_{(\beta)}}dy_3, \quad C^{2jb}_{an\alpha\beta} = \int_{-H/2}^{H/2} L_jL_bC_{an\alpha\beta}\frac{\mathcal{H}_{(n)}}{H_{(\alpha)}}dy_3 \\ & C^{3jbd}_{an\alpha\beta} = \int_{-H/2}^{H/2} L_jL_bL_dC_{an\alpha\beta}\frac{\mathcal{H}_{(n)}}{H_{(\alpha)}H_{(\beta)}}dy_3, C^{4jib}_{an\alpha\beta} = \int_{-H/2}^{H/2} L_jL_iL_bC_{an\alpha\beta}\frac{\mathcal{H}_{(n)}}{H_{(a)}H_{(\beta)}}dy_3 \\ & C^{5jib}_{an\alpha\beta} = \int_{-H/2}^{H/2} L_jL_iL_bC_{an\alpha\beta}\frac{\mathcal{H}_{(n)}}{H_{(a)}H_{(\alpha)}}dy_3, \quad C^{6jibd}_{an\alpha\beta} = \int_{-H/2}^{H/2} L_jL_iL_bL_dC_{an\alpha\beta}\frac{\mathcal{H}_{(n)}}{H_{(a)}H_{(\alpha)}H_{(\beta)}}dy_3 \end{aligned} \tag{28}$$

Here, indices i, j, b, d = 0, 1, 2, 3 and other indices take values 1 and 3. The non-zero terms of M^j_{mn} for a beam are listed in Appendix A.

The true stress or the Cauchy stress, $\boldsymbol{\sigma}$, is related to the 1st Piola–Kirchhoff stress by

$$\boldsymbol{\sigma} = \frac{1}{J}\boldsymbol{TF}^T, \tag{29}$$

where J is the determinant of the deformation gradient $\boldsymbol{F}$.

We are unable to analytically solve the above formulated nonlinear problem; thus we analyze it numerically.

3. Numerical solution

3.1. Weak formulation

Let Θ^j_1 and Θ^j_3 be smooth functions of $y_1 \epsilon [0, \mathcal{L}]$. We take the inner product of both sides of Eqs. (17.a) and (17.b) with Θ^j_1 and Θ^j_3, respectively, integrate the resulting equations with respect to y_1 on $[0, \mathcal{L}]$, and then integrate by parts to arrive at the following equations:

$$\begin{aligned} \int_0^{\mathcal{L}} \Theta^j_1(A_{ji}\ddot{u}_{1i})dy_1 = {} & \int_0^{\mathcal{L}}\left(-\frac{\partial\Theta^j_1}{\partial y_1}M^j_{11} + \Theta^j_1\left(\frac{1}{R}M^j_{31} + \bar{f}^j_1 + B^j_{13} - D_{ji}M^i_{13}\right)\right)dy_1 B^j_{11} \\ & \int_0^{\mathcal{L}} \Theta^j_3(A_{ji}\ddot{u}_{3i})dy_1 \\ = {} & \int_0^{\mathcal{L}}\left(-\frac{\partial\Theta^j_3}{\partial y_1}M^j_{31} + \Theta^j_3\left(\bar{f}^j_3 + B^j_{33} - D_{ji}M^i_{33} - \frac{1}{R}M^i_{11}\right)\right)dy_1 + B^j_{31} \end{aligned} \tag{30}$$

where

$$\begin{aligned} B^j_{11} &= \Theta^j_1(\mathcal{L})M^j_{11}(\mathcal{L}) - \Theta^j_1(0)M^j_{11}(0), \\ B^j_{31} &= \Theta^j_3(\mathcal{L})M^j_{31}(\mathcal{L}) - \Theta^j_3(0)M^j_{31}(0) \end{aligned} \tag{31}$$

Here indices i, j = 0, 1, 2, 3. If one thinks of Θ^j_1 and Θ^j_3 as virtual displacements that vanish at boundary points where displacements are prescribed, then Eq. (30) states the principle of virtual work. Alternatively, Eq. (30) expresses a weak formulation of the problem since it involves first-order derivatives of u_1 and u_3 with respect to y_1 whereas the PDEs (17) have second-order derivatives of u_1 and u_3 with respect to y_1. Since T_{11}, T_{13}, T_{31} and T_{33} are nonlinear functions of displacement gradients, Eq. (30) is nonlinear in u_1 and u_3.

3.2. Derivation of ordinary differential equations

We discretize the curve along the y_1-axis into one-dimensional finite elements (FEs) of not necessarily the same length. Let there be N nodes on this curve and $\Psi_1(y_1), \Psi_2(y_1), \ldots, \Psi_N(y_1)$ be the FE basis functions. We write

$$u_{\alpha j}(y_1, t) = \sum_{i=1}^{N}\Psi_i(y_1)\tilde{d}_{\alpha ij}(t), \qquad j = 0,1,2,3; \quad \alpha = 1,3. \tag{32}$$

Substitution from Eq. (32) into Eq. (8) gives

$$u_\alpha(y_1, y_3, t) = \sum_{j=0}^{3}L_j(y_3)\sum_{i=1}^{N}\Psi_i(y_1)\tilde{d}_{\alpha ij}(\ t), \qquad j = 0,1,2,3; \quad \alpha = 1,3 \tag{33}$$

Thus for N nodes along the y_1-axis with node 1 at y_1 = 0, we have 8 N unknown functions $\tilde{d}_{\alpha ij}(t), \alpha = 1,3; i = 1,2,\ldots,N; j = 0,1,2,3$. We write these as the 8 N-dimensional vector $\boldsymbol{d}(t)$, and the displacement field $u_{\alpha j}(y_1, t)$ as 8-dimensional vector $\tilde{\boldsymbol{u}}(y_1, t)$. These can be written as

$$\begin{aligned} \{\tilde{\boldsymbol{u}}(y_1, t)\} &= [\emptyset(y_1)]\{\boldsymbol{d}(t)\} \\ \{\tilde{\boldsymbol{u}}(y_1, t)\} &= \{u_{10}\ u_{11}\ u_{12}\ u_{13}\ u_{30}\ u_{31}\ u_{32}\ u_{33}\}^T \end{aligned} \tag{34}$$

where $[\emptyset]$ is 8×8 N matrix and $\{\boldsymbol{d}\}$ is 8 N $\times$ 1 matrix. In index notation, Eq. (34) becomes

$$\tilde{u}_\beta(y_1, t) = \emptyset_{\beta j}(y_1)d_j(t), \qquad \beta = 1,2,\ldots,8; \quad j = 1,2,\ldots,8N \tag{35}$$

We can also write the displacement fields $u_1(y_1, y_3, t)$ and $u_3(y_1, y_3, t)$ as

$$\begin{Bmatrix} u_1(y_1, y_3, t) \\ u_3(y_1, y_3, t) \end{Bmatrix} = [\varphi(y_3)][\emptyset(y_1)]\{\boldsymbol{d}(t)\} = [\Phi(y_1, y_3)]\{\boldsymbol{d}(t)\} \tag{36}$$

where $[\varphi(y_3)]$ is 2×8 matrix, $[\emptyset\ (y_1)]$ is 8×8 N matrix and $[\Phi]$ is 2×8 N matrix.

We use the Galerkin formulation and take the same basis functions for the test functions Θ_1^j, Θ_3^j as those for the trial solutions u_{1j}, u_{3j}; e.g., see Eq. (32). That is

$$\Theta_\alpha^j(y_1) = \sum_{i=1}^{N} \Psi_i(y_1) c_{\alpha i}^j, \qquad \alpha = 1,3; \quad j = 0,1,2,3 \tag{37}$$

where $c_{\alpha i}^j$ are constants.

Substitution from Eqs. (35) and (37) into Eq. (30) and requiring that the resulting equations hold for all values of constants $c_{\alpha i}^j$ gives the following set of coupled nonlinear ordinary differential equations (ODEs).

$$\boldsymbol{M}\ddot{\boldsymbol{d}} = \boldsymbol{F}^{ext} - \boldsymbol{F}^{int}(\boldsymbol{d}), \tag{38}$$

where

$$\boldsymbol{M} = \int_0^{\mathcal{L}} [\emptyset(y_1)]^{\mathrm{T}} [\overline{A}] [\emptyset(y_1)] dy_1, \quad [\overline{A}] = \begin{bmatrix} A & 0 \\ 0 & A \end{bmatrix}$$

$$\boldsymbol{F}^{ext} = \int_0^{\mathcal{L}} [\emptyset(y_1)]^{\mathrm{T}} \begin{Bmatrix} vec\left(\bar{f}_1^j + B_{13}^j\right) \\ vec\left(\bar{f}_3^j + B_{33}^j\right) \end{Bmatrix} dy_1 + [\emptyset(\mathcal{L})]^{\mathrm{T}} \begin{Bmatrix} vec\left(M_{11}^j(\mathcal{L})\right) \\ vec\left(M_{31}^j(\mathcal{L})\right) \end{Bmatrix} - [\emptyset(0)]^{\mathrm{T}} \begin{Bmatrix} vec\left(M_{11}^j(0)\right) \\ vec\left(M_{31}^j(0)\right) \end{Bmatrix}$$

$$\boldsymbol{F}^{int} = \int_0^{\mathcal{L}} [BL1]^T \left\{ vec\left(M_{11}^j\right) \;\; vec\left(M_{31}^j\right) \;\; vec\left(D_{ji} M_{13}^i - \tfrac{1}{R} M_{31}^j\right) \;\; vec\left(D_{ji} M_{33}^i + \tfrac{1}{R} M_{11}^j\right) \right\}^T dy_1$$

$$[BL1] = \begin{bmatrix} diag\left(\frac{\partial}{\partial y_1}\right) & 0 \\ 0 & diag\left(\frac{\partial}{\partial y_1}\right) \\ diag(1) & 0 \\ 0 & diag(1) \end{bmatrix} [\emptyset(y_1)], \quad diag(\mathrm{f}) = \mathrm{diagonal}\{\mathrm{f}\ \mathrm{f}\ \mathrm{f}\ \mathrm{f}\} \tag{39}$$

$$diag(\mathrm{f}^j) = \mathrm{diagonal}(\mathrm{f}^0\ \mathrm{f}^1\ \ \mathrm{f}^2\ \mathrm{f}^3), vec(\mathrm{f}^j) = \{\mathrm{f}^0\ \ \mathrm{f}^1\ \mathrm{f}^2\ \mathrm{f}^3\}$$

Here $\boldsymbol{M} = \boldsymbol{M}^T$ is the consistent mass matrix, $\boldsymbol{F}^{ext}$ represents the generalized 8 N-dimensional nodal force ($\boldsymbol{F}^{ext}$ is 8 N × 1 matrix) equivalent to the externally applied surface tractions on boundaries and the body force (e.g., gravity). The 8 N-dimensional vector $\boldsymbol{F}^{int}$ represents forces due to internal stresses, and is a nonlinear function of the generalized nodal displacement $\boldsymbol{d}$ since stresses T_{11}, T_{13}, T_{31} and T_{33} are nonlinear functions of u_1 and u_3. However, the weak formulation involves only first-order derivatives of generalized displacements. Thus lower order basis functions can be used to numerically analyze the problem. For example, for plates made of linear elastic materials, Qian et al. [38,44–49], Xiao et al. [39,50–52] and Batra and Aimmanee [53] have used, respectively, basis functions derived by the moving least squares approximation, radial basis functions in meshless methods and the finite element method to study transient deformations of thick plates using Kth order shear and normal deformable plate theory. Here we consider material and geometric nonlinearities and use the TSNDT.

We now find initial values of $\boldsymbol{d}(0)$ from $\boldsymbol{u}$ $(y_1, y_3, 0)$. Substituting time $t = 0$ in Eq. (36) and using Eq. (12.c) we get

$$\begin{Bmatrix} u_1(y_1, y_3, 0) \\ u_3(y_1, y_3, 0) \end{Bmatrix} = [\Phi(y_1, y_3)]\{d(0)\} = \begin{Bmatrix} u_1^0(y_1, y_3) \\ u_3^0(y_1, y_3) \end{Bmatrix} \tag{40}$$

Premultiplying both sides of Eq. (40) by $\rho_0[\Phi]^T(y_1, y_3)$ and integrating the result over Ω_0 yield

$$\boldsymbol{M}\boldsymbol{d}^0 = \boldsymbol{F}^0, \;\; \boldsymbol{d}^0 = d(0), \quad \boldsymbol{F}^0 = \int_{\Omega_0} \rho_0 [\Phi]^T \begin{Bmatrix} u_1^0 \\ u_3^0 \end{Bmatrix} H_1 dy_1 dy_3 \tag{41}$$

The solution of Eq. (41) gives $\boldsymbol{d}^0$. We follow a similar procedure to find $\dot{\boldsymbol{d}}^0$. The natural boundary conditions (12.e) are included in Eq. (17). The essential boundary conditions (12.f) in terms of $\tilde{d}_{\alpha ij}(t)$ are satisfied during the solution of Eq. (38).

If the edge, $y_1 = 0$, of the beam is simply supported, clamped or free, boundary conditions there are, respectively, given by Eqs. (42–44).

$$\tilde{d}_{31j}(0,t) = 0, \qquad j = 0,1,2,3, \quad M_{11}^j(0,t) = 0, \quad j = 0,1,2,3; \tag{42.a, b, c}$$

$$\tilde{d}_{\alpha 1j}(t) = 0, \qquad j = 0,1,2,3; \quad \alpha = 1,3; \tag{43}$$

$$M_{11}^j(0,t) = 0, \qquad M_{31}^j(0,t) = 0, \quad j = 0,1,2,3. \tag{44}$$

That is, at a simply supported edge the transverse displacement and moments about the y_2-axis of tractions due to T_{11} of orders 0 through 3 vanish. The boundary condition (42.b) eliminates rigid body translation in the y_1-direction and is needed only if the other edge is either simply supported or free. At a clamped edge both the axial and the transverse displacements identically vanish. At a free edge, moments about the y_2-axis of orders 0 through 3 of tractions due to T_{11} and the transverse shear forces due to T_{31} vanish.

We note that the FE formulations for the Euler–Bernoulli and the Timoshenko beam theories involve two unknowns at a node, namely, the transverse displacement and the slope. Here, at a node we have eight unknowns which may be associated with the displacement, the slope, the curvature, and the curvature gradient. The anticipated benefit of considering more unknowns at a node is improved solution for the transverse normal, the transverse shear and axial deformations of the beam. For a continuous elastodynamic problem, there are two unknowns at a node. Thus the numbers of degrees of freedom for the TSNDT and the 2-D elasticity problem would be the same if we take four nodes in the y_3-direction for the elasticity problem. The main benefit of using the TSNDT is savings in not generating a 2-D FE mesh. In the continuous problem one can approximate displacements in the y_3-direction either with piecewise affine functions or piecewise quadratic functions or a cubic polynomial; the last case corresponds to the displacement field assumed in the TSNDT. Through numerical experiments, we will show in Section 5 that even for thick beams the TSNDT gives as accurate results as those obtained from the analysis of the continuum problem.

3.3. Solution of nonlinear ODEs

We use the conditionally stable central-difference method to integrate the coupled nonlinear ODEs (38). That is, with the notation

$$\boldsymbol{d}^{n+1} = \boldsymbol{d}(t_{n+1}), \tag{45}$$

we have

$$\boldsymbol{d}^{n+1} = \boldsymbol{d}^n + \Delta t \dot{\boldsymbol{d}}^n + \frac{\Delta t^2}{2} \ddot{\boldsymbol{d}}^n, \qquad \ddot{\boldsymbol{d}}^{n+1} = \boldsymbol{M}^{-1}[\boldsymbol{F}^{ext}(t_{n+1}) - \boldsymbol{F}^{int}(\boldsymbol{d}^{n+1})] \tag{46.a, b}$$

$$\dot{\boldsymbol{d}}^{n+1} = \dot{\boldsymbol{d}}^n + \frac{\Delta t}{2}(\ddot{\boldsymbol{d}}^{n+1} + \ddot{\boldsymbol{d}}^n) \tag{46.c}$$

The critical time step size to compute a stable solution is determined by finding the maximum frequency, ω_{max}, of free vibrations and taking $\Delta t \leqslant \Delta t_{crit}$, $\Delta t_{crit} = 2/\omega_{max}$. Ideally, ω_{max} should be found after every time step since frequencies of a structure change as it is deformed. The accuracy of the solution can be improved by taking $\Delta t \ll \Delta\, t_{crit}$ but at the cost of increasing the computational time.

Results presented in Section 5 have been computed with a consistent mass matrix and $\Delta t = 0.9\Delta t_{crit}$ for a linear problem but $\Delta t = 0.5\Delta t_{crit}$ for a nonlinear problem. For the nonlinear problems, ω_{max} found from analyzing frequencies of the undeformed beam is used to ascertain Δt_{crit}.

For a static problem, we use the modified Newton–Raphson method. That is, we iteratively solve

$$\boldsymbol{F}^{int}(\boldsymbol{d}) = \boldsymbol{F}^{ext}, \tag{47}$$

by first writing it as

$$\boldsymbol{K}\Delta\boldsymbol{d} = -(\boldsymbol{F}^{int}(\bar{\boldsymbol{d}}) - \boldsymbol{F}^{ext}),\ \boldsymbol{K} = \left.\frac{\partial \boldsymbol{F}^{int}}{\partial \boldsymbol{d}}\right|_{\boldsymbol{d}=\bar{\boldsymbol{d}}},\ \boldsymbol{d} = \bar{\boldsymbol{d}} + \Delta\boldsymbol{d} \tag{48.a}$$

$$\boldsymbol{K} = \int_0^{\mathcal{L}} \rho_0 [\mathrm{BL1}]^T [\mathbb{Q}][\kappa][\mathrm{BL2}] dy_1 \tag{48.b}$$

$$[BL2] = \begin{bmatrix} diag\left(\frac{\partial}{\partial y_1}\right) & diag\left(\frac{1}{R}\right) \\ 0 & D^T \\ D^T & 0 \\ diag\left(\frac{1}{R}\right) & diag\left(\frac{\partial}{\partial y_1}\right) \end{bmatrix} [\emptyset(y_1)] \tag{48.c}$$

$$[\kappa] = \begin{bmatrix} \kappa_{11} & \kappa_{12} & \kappa_{13} & \kappa_{14} \\ \kappa_{21} & \kappa_{22} & \kappa_{23} & \kappa_{24} \\ \kappa_{31} & \kappa_{32} & \kappa_{33} & \kappa_{34} \\ \kappa_{41} & \kappa_{42} & \kappa_{43} & \kappa_{44} \end{bmatrix}, [\mathbb{Q}] = \begin{bmatrix} \mathbb{Q}_{11} & \mathbb{Q}_{12} & \mathbb{Q}_{13} & \mathbb{Q}_{14} \\ \mathbb{Q}_{21} & \mathbb{Q}_{22} & \mathbb{Q}_{23} & \mathbb{Q}_{24} \\ \mathbb{Q}_{31} & \mathbb{Q}_{32} & \mathbb{Q}_{33} & \mathbb{Q}_{34} \\ \mathbb{Q}_{41} & \mathbb{Q}_{42} & \mathbb{Q}_{43} & \mathbb{Q}_{44} \end{bmatrix} \tag{48.d}$$

Here each term of $[\kappa]$ and $[\mathbb{Q}]$ like $\kappa_{11}, \mathbb{Q}_{11}$ etc. is 4×4 matrix. The non-zero terms of $[\mathbb{Q}]$ are

$$\mathbb{Q}^{jb}_{11} = \delta_{jb}, \quad \mathbb{Q}^{jb}_{23} = \delta_{jb}, \quad \mathbb{Q}^{jb}_{33} = D_{jb}, \quad \mathbb{Q}^{jb}_{34} = -\frac{1}{R}\delta_{jb},$$
$$\mathbb{Q}^{jb}_{42} = D_{jb}, \quad \mathbb{Q}^{jb}_{41} = \frac{1}{R}\delta_{jb} \tag{49}$$

Here j, $b = 0, 1, 2, 3$, D_{jb} is specified in Eq. (8.e). Expressions for elements of $[\kappa]$ are listed in Appendix B.

The iterative process is terminated when the norm of the residual load vector, $\bar{R}$, defined by

$$\boldsymbol{R} = \boldsymbol{F}^{int}(\boldsymbol{d}) - \boldsymbol{F}^{ext}, \quad \bar{R} = max(|\boldsymbol{R}|)N/Sum(|\boldsymbol{F}^{ext}|) \tag{50.a, b}$$

is less than the prescribed value. During a given load step the stiffness matrix is evaluated only at the start of the load step. In Eq. (50) N equals the number of degrees of freedom.

4. Curved laminated beam

For simplicity we consider a 3-layer curved laminated beam, and denote displacements of a point in the top, the central, and the bottom layers by superscripts t, c and b, respectively. With the origin of the curvilinear coordinate axes located at the geometric centroid of the rectangular cross-section (e.g., see Fig. 2), we assume the following displacement field in the beam.

$$u^c_\alpha(y_1, y_3, t) = \sum_{i=0}^{3} (y_3)^i l^c_{\alpha i}(y_1, t), \quad \alpha = 1, 3, |y_3| \leqslant H^c \tag{51.a}$$

$$u^t_\alpha(y_1, y_3, t) = u^c_\alpha(y_1, H^c, t) + \sum_{i=0}^{3} ((y_3)^i - (H^c)^i) l^t_{\alpha i}(y_1, t),$$
$$\alpha = 1, 3, H^c < y_3 < H^c + H^t \tag{51.b}$$

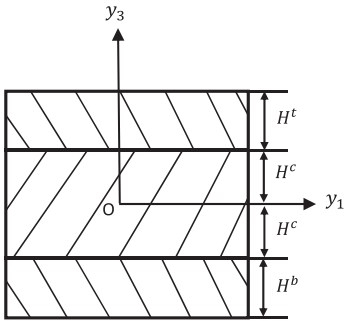

Fig. 2. Cross-section of a 3-layer beam.

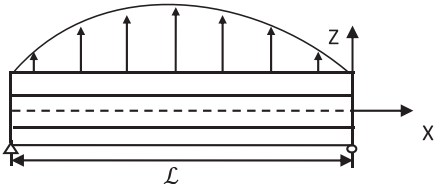

Fig. 3. Schematic sketch of the problem studied.

Table 1
Comparison of beam centroid deflection $\underline{w}(\frac{\ell}{2}, 0)$ (82 uniform elements with piecewise linear basis functions used to compute results with the TSNDT).

L/H	4	10	20	50	100
TSNDT	2.886	0.9312	0.6170	0.5268	0.5138
Elasticity	2.887	0.9316	0.6173	0.5270	0.5140
Difference (%)	0.0346	0.0429	0.0486	0.0380	0.0389

$$u^b_\alpha(y_1, y_3, t) = u^c_\alpha(y_1, -H^c, t) + \sum_{i=0}^{3} ((y_3)^i - (-H^c)^i) l^b_{\alpha i}(y_1, t),$$
$$\alpha = 1, 3, \ -(H^b + H^c) \leqslant y_3 \leqslant -H^c \tag{51.c}$$

In Eq. (51) $2H^c$ equals the height of the central beam, and H^t and H^b heights of the top and the bottom beams, respectively. The assumed displacement field (51) is continuous across interfaces between the central and the top and the bottom beams. The continuity of surface tractions across these interfaces is implicitly satisfied during the derivation of the weak formulation of the problem.

For each displacement component, Eqs. 51.a, 51.b, and 51.c have four unknowns for the top, the central and the bottom layers. Thus in the TSNDT the number of degrees or unknowns for N nodes on the centroidal axis equals 24 N. For studying plane strain deformations of a laminated beam composed of three plies using 4-node quadrilateral elements with three elements across the thickness in each ply, the number of degrees of freedom for N nodes along the y_1-axis will equal 20 N.

The governing equations and the weak formulation derived, respectively, in Section 2 and subsection 3.1 remain unaffected by the number of plies. However, the displacement function L_j and the matrix $[D]$ need to be changed, and the material properties of the pertinent layer are used while evaluating integrals in Eq. (28).

5. Results for example problems

5.1. Linear problems

When analyzing linear elastic problems, we omit all nonlinear terms in expressions for the strain components, and note that differences among the three stress tensors, namely, the 1st and the

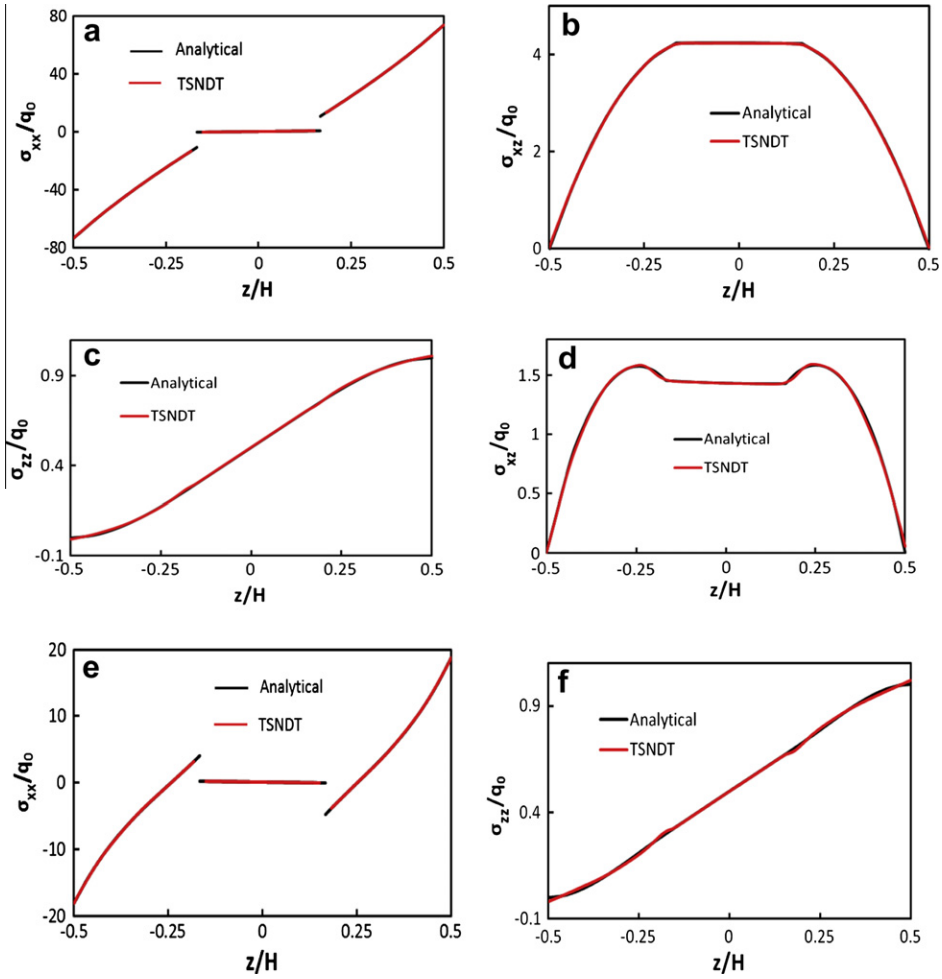

Fig. 4. Comparison of through-the-thickness distributions of stresses derived from the analytical solution based on the linear elasticity theory and the TSNDT solution for (0°/90°/0°) laminates; black curves represent the elasticity solution and red curves the TSNDT solution; (a) σ_{xx} at $x = \mathcal{L}/2$ for $\mathcal{L}/H = 10$; difference, $\bar{\eta} = 0.062\%$; (b) σ_{xz} at $x = 0$ for $\mathcal{L}/H = 10$; difference, $\bar{\eta} = 0.146\%$; (c) σ_{zz} at $x = \mathcal{L}/2$ for $\mathcal{L}/H = 10$; difference, $\bar{\eta} = 0.439\%$; (d) σ_{xz} at $x = 0$ for $\mathcal{L}/H = 4$; difference, $\bar{\eta} = 0.742\%$; (e) σ_{xx} at $x = \mathcal{L}/2$ for $\mathcal{L}/H = 4$; difference, $\bar{\eta} = 0.439\%$; and (f) σ_{zz} at $x = \mathcal{L}/2$ for $\mathcal{L}/H = 4$; difference, $\bar{\eta} = 0.941\%$. (For interpretation of the references to color in this figure legend, the reader is referred to the web version of this article.)

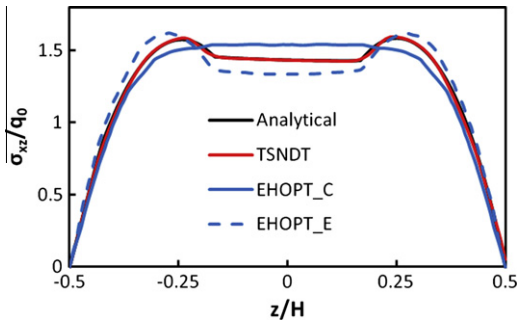

Fig. 5. Comparison of through-the-thickness variation of σ_{xz} at $x = 0$ for $\mathcal{L}/H = 4$ using the TSNDT, the EHOPT_C and the EHOPT_E; in EHOPT_C and EHOPT_E stresses are computed, respectively, by using constitutive equations and by integrating equilibrium equations.

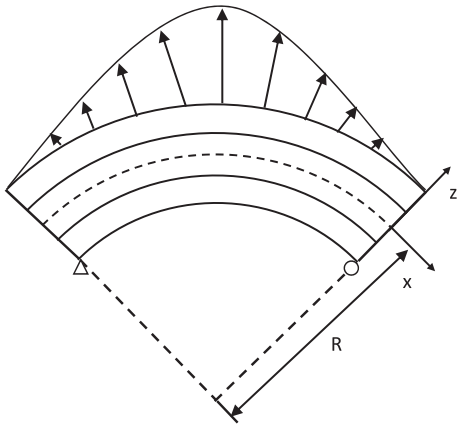

Fig. 6. Schematic sketch of a 3-layer laminated curved beam loaded by a sinusoidal normal traction on the top surface.

2nd Piola–Kirchhoff and the Cauchy are negligible. Also, we use the more common notation and replace y_1 and y_3 by x and z, respectively, and u_1 and u_3 by u and w, respectively. Unless otherwise stated, integrals in Eqs. (38) and (28) are numerically evaluated, respectively, by using 1 Gauss point in the x-direction, and 5 in each layer in the z-direction.

5.1.1. Static infinitesimal deformations of straight laminated beam

We study static infinitesimal deformations of a simply supported (0°/90°/0°) straight beam loaded by a uniformly distributed normal traction, $q = q_0 sin(\frac{\pi x}{\mathcal{L}})$, on the top surface with the bottom

Table 2
Comparison of the analytical solution of the shell centroid deflection, $\underline{w}(\frac{\mathcal{L}}{2},0)$, with those obtained by using different meshes and the number of integration points in the thick shell theory (the number of integration points in the z-direction are for each layer and are used to numerically evaluate integrals in Eq. (28)).

χ	Number of integration points (x, z)	21 Nodes	41 Nodes	81 Nodes	161 Nodes	Exact[41]
4	1,5	0.457	0.458	0.458	–	0.457
	3,5	0.446	0.455	0.457	–	
10	1,5	0.143	0.144	0.144	–	0.144
	3,5	0.136	0.142	0.144	–	
50	1,5	0.0804	0.0807	0.0808	–	0.0808
	3,5	–	0.0666	0.0768	0.0798	
100	1,5	0.0782	0.0785	0.0785	–	0.0787
	3,5	–	0.0429	0.0653	0.0747	

Table 3
Comparison of the centroid deflection, $\underline{w}(\frac{\mathcal{L}}{2},0)$, from the straight beam and the thick shell theories computed with different number of nodes in the x-direction.

χ		5 Nodes	11 Nodes	21 Nodes	41 Nodes	Exact [41]
4	Thick shell	0.433	0.454	0.457	0.458	0.457
	Straight beam	0.333	0.385	0.397	0.405	
10	Thick shell	0.132	0.142	0.143	0.144	0.144
	Straight beam	0.109	0.127	0.132	0.135	
50	Thick shell	0.0710	0.0792	0.0804	0.0807	0.0808
	Straight beam	0.0600	0.0735	0.0768	0.0786	
100	Thick shell	0.0688	0.0770	0.0782	0.0785	0.0787
	Straight beam	0.0582	0.0718	0.0750	0.0767	

Table 4
Comparison of the deflection $\underline{w}(\frac{\mathcal{L}}{2},0)$ for the thin shell, the thick shell and the straight beam theories computed using 161 nodes for the straight beam theory when $\chi = 50$ and 100, and 81 nodes for all other theories and other values of χ.

χ	4	10	50	100
Exact [41]	0.457	0.144	0.0808	0.0787
TSNDT-Thick shell	0.458	0.144	0.0808	0.0785
TSNDT-Thin shell	0.412	0.137	0.0800	0.0781
TSNDT-Straight beam	0.409	0.136	0.0798	0.0779
CST	0.0781	0.0777	0.0776	0.0776
FSDST [42]	0.289	0.113	0.0786	0.0776
HSDST [42]	0.382	0.128	0.0793	0.0777
EHOST [36]	0.455	0.143	0.0808	0.0787
Zig–zag [43]	0.441	0.143	0.0810	0.0788

Table 5
Comparison of stress $\underline{\sigma}_{xx}(\frac{\mathcal{L}}{2},\mp\frac{H}{2})$ from different theories; 161 nodes in the x-direction for the straight beam theory when $\chi = 50$ and 100, and 81 nodes for all other cases.

χ	4	10	50	100
Exact [41]	−1.772	−0.995	−0.798	−0.786
	1.367	0.897	0.782	0.781
TSNDT-Thick shell	−1.772	−0.995	−0.798	−0.786
	1.367	0.897	0.783	0.779
TSNDT-Thin shell	−1.378	−0.905	−0.784	−0.779
	1.398	0.895	0.781	0.778
TSNDT-Straight beam	−1.371	−0.901	−0.780	−0.776
	1.393	0.892	0.778	0.775
EHOST [36]	−1.702	−0.967	−0.794	−0.785
	1.599	0.928	0.786	0.780
Zig–zag [43]	−1.792	−1.003	−0.799	−0.787
	1.350	0.894	0.783	0.779

Table 6
Comparison of stress $\underline{\sigma}_{xz}(0,0)$ from different theories; 161 nodes in the x-direction for the straight beam theory when $\chi = 50$ and 100, and 81 nodes for all other cases.

χ	4	10	50	100
Exact [41]	0.476	0.525	0.526	0.523
TSNDT-Thick shell	0.476	0.525	0.525	0.523
TSNDT-Thin shell	0.427	0.501	0.520	0.520
TSNDT-Straight beam	0.425	0.498	0.518	0.519
EHOST [36]	0.516	0.545	0.537	0.535
Zig–zag [43]	0.447	0.524	0.525	0.524

surface traction free; a schematic sketch of the problem studied is shown in Fig. 3. Each layer is of the same thickness.

Values assigned to material parameters, taken from Pagano [40] who solved the problem analytically, are

$$E_L = 172\ \text{GPa},\ E_T = 6.9\ \text{GPa},\ G_{LT} = 3.4\ \text{GPa},\quad G_{TT} = 1.4\ \text{GPa},\ \nu_{TL} = \nu_{TT} = 0.25 \tag{52}$$

Here subscript L denotes the direction parallel to the fiber, subscript T the transverse direction, and ν is Poisson's ratio; i.e., E_T and E_L are elastic moduli in the transverse and the longitudinal directions, respectively, and G_{LT} is the shear modulus.

The percentage error, $\bar{\eta}$, in the TSNDT solution for variable σ is defined by

$$\bar{\eta} = 100\left(\int_0^{\mathcal{L}} |\sigma_{\text{TSNDT}} - \sigma_{ana}|dx\right) \Big/ \int_0^{\mathcal{L}} |\sigma_{ana}|dx \tag{53}$$

where subscripts TSNDT and *ana* denote, respectively, numerical results computed by using the TSNDT and the analytical approach. The deflection,w, is normalized by

$$\underline{w} = \frac{100E_T H^3 w}{q_0 \mathcal{L}^4} \tag{54}$$

The normalized mid-point deflection of the beam from the TSNDT and the analytical approach as well as the percentage difference between the two results is listed in Table 1. It is clear that for $\mathcal{L}/H$ varying from 4 to 100 the mid-point deflection computed using the TSNDT differs from that found using the analytical approach by 0.04%. For $\mathcal{L}/H = 4$ and 10, we have exhibited in Fig. 4a–f through-the-thickness variations of the axial, the transverse normal and the transverse shear stresses computed using the TSNDT and the analytical approach. Stresses using the TSNDT are found from the constitutive relations and the displacement fields. The difference $\bar{\eta}$ between stresses from the two approaches is less than 1% implying that the TSNDT gives accurate values of stresses including those of the transverse shear and the transverse normal stresses without using any stress recovery technique. We note that the transverse normal and the transverse shear stresses computed with the TSNDT are continuous across interfaces between adjoining plies. In Fig. 5 we have compared the presently computed values of the transverse shear stress for a beam with $\mathcal{L}/H = 4$ with those given in [21] using an efficient higher order plate theory, EHOPT, that assumes a combination of zig–zag and a cubic variation in the z-direction of in-plane displacements. The transverse shear stresses denoted as EHOPT-C and EHOPT-E are computed, respectively, by using the constitutive equations and by integrating equilibrium equations. It is evident that the present results obtained without using any stress recovery technique are closer to the analytical solution than those derived from the EHOPT using the post-processing method.

5.1.2. Static infinitesimal deformations of curved laminated beam

The second problem studied is that of a simply supported (0°/90°/0°) beam of constant radius of curvature, $R = 25.4$ cm, length $\mathcal{L} = R\pi/3$, ply thickness = H/3, subjected to sinusoidal normal traction q on the top surface as shown in Fig. 6, and material properties

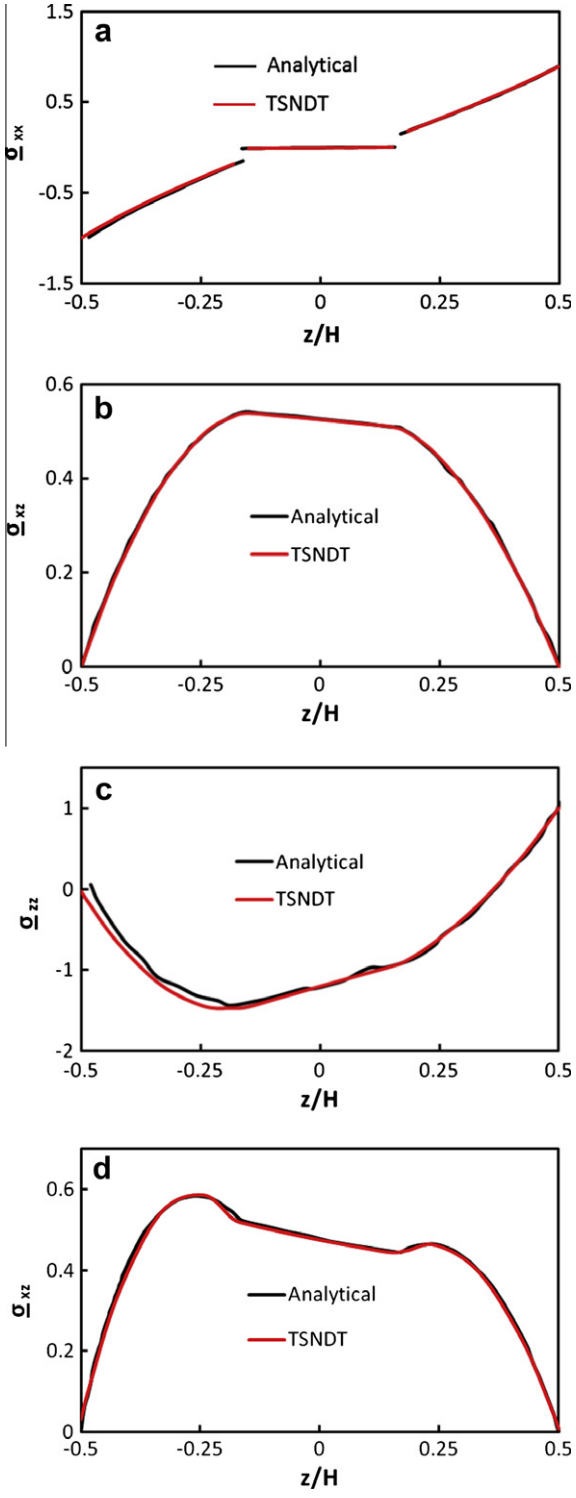

Fig. 7. Comparison of through-the-thickness variation of stresses found from the analytical and the TSNDT solutions; black curve - analytical solution, red curve - TSNDT (thick shell theory), (a) $\underline{\sigma}_{xx}$ at $x = \mathcal{L}/2$ when $R/H = 10$; difference, $\bar{\eta} = 2.37\%$, (b)$\underline{\sigma}_{xz}$ at $x = 0$ when $R/H = 10$; difference, $\bar{\eta} = 1.18\%$, (c) $\underline{\sigma}_{zz}$ at $x = \mathcal{L}/2$ when $R/H = 10$; difference, $\bar{\eta} = 5.17\%$, and (d) $\underline{\sigma}_{xz}$ at $x = 0$ when $R/H = 4$; difference, $\bar{\eta} = 1.01\%$. (For interpretation of the references to color in this figure legend, the reader is referred to the web version of this article.)

given in Eq. (52). Results are presented in terms of the following non-dimensional variables:

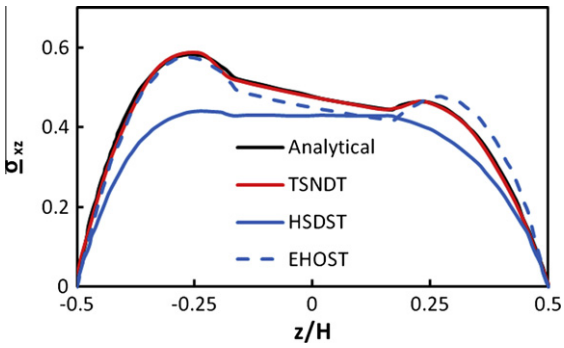

Fig. 8. Through-the-thickness variation of $\underline{\sigma}_{xz}$ at $x = 0$ when $R/H = 4$ for different theories, shear stresses in the HSDST and the EHOST are derived by integrating the equilibrium equations.

$$\underline{w} = \frac{10E_T w}{q_0 H \chi^4}, \quad \underline{\sigma}_{xx} = \frac{\sigma_{xx}}{q_0 \chi^2}, \quad \underline{\sigma}_{xz} = \frac{\sigma_{xz}}{q_0 \chi}, \quad \underline{\sigma}_{zz} = \frac{\sigma_{zz}}{q_0}, \quad \chi = R/H \tag{55}$$

The analytical results obtained by digitizing plots in [41] are compared with those computed with the TSNDT, the CST [41], the FSDST [42], the HSDST [42], the EHOST [36], and the zig–zag [43] shell theory. The shell theory discussed in Section 2 that considers (does not consider) the variation of the radius of curvature through the shell thickness is called "thick (thin) shell theory". Deformations of a curved beam can also be analyzed by dividing it into small segments and approximating each segment as a straight line; the analysis based on this technique is called the "straight beam theory". This approach does not consider through-the-thickness variation of the radius of curvature.

The centroidal deflections and stresses at two points obtained with different theories are compared with the analytical solution in Tables 2–6. The TSNDT results presented in Table 2 with different number of integration points in the x- and the z-directions for evaluating integrals in Eqs. (38) and (28), respectively, suggest that using 1 Gauss point in the x-direction in each FE and five in each layer in the z-direction provides sufficiently accurate results for χ between 4 and 100. Unless otherwise specified, results presented below have been computed with 1 Gauss point in the x-direction in each 1-D FE. Values of centroidal deflection from the thick shell and the straight beam theories listed in Table 3 suggest that the deflection using the thick shell theory converges significantly faster than that derived from the straight beam theory.

For $\chi = 4$, 10, 50 and 100, converged values of stresses at critical points based on different shell theories are compared with their values from the analytical solution in Tables 4–6. For $\chi = 50$ and 100, all theories give very good values of stresses. However, for $\chi = 4$ and 10, the thick shell theory gives superior results than those obtained with the other shell theories considered here. For $\chi = 4$ and 10, the through-the-thickness variations of stresses found with the thick shell TSNDT are compared in Figs. 7 and 8 with those from the analytical solution of Ren [41]. The maximum difference in the two values of a stress component is about 2% except for 5.1% for $\underline{\sigma}_{zz}$ when $\chi = 10$ which most likely is due to digitization errors as the plot of $\underline{\sigma}_{zz}$ in [41] is not clear. Results presented in Section 5.5 will show that the thick shell TSNDT predicts $\underline{\sigma}_{zz}$ for $\chi = 10$ in agreement with that obtained using the commercial FE software, ABAQUS. In Fig. 8 we have exhibited through-the-thickness variation of the transverse shear stress found from three shell theories and the analytical solution of the boundary value problem. The three shell theories predict continuous variation of $\underline{\sigma}_{xz}$, and results from the thick shell TSNDT are in better

Table 7
For different node numbers along the x-axis in the TSNDT and for different FE meshes in ABAQUS, values at critical points of the centroidal deflection and stresses from the linear and the nonlinear theories.

L/H		Nodes	Linear			Nonlinear		
			w/H $(\mathcal{L}/2,0)$	σ_{xx}/q_0 $(\mathcal{L}/2,-H/2)$	σ_{xz}/q_0 $(\mathcal{L}/4,0)$	w/H $(\mathcal{L}/2,0)$	σ_{xx}/q_0 $(\mathcal{L}/2,-H/2)$	σ_{xz}/q_0 $(\mathcal{L}/4,0)$
	TSNDT	21	0.8043	−96.3	7.851	0.6254	−57.49	6.910
		61	0.8147	−100.4	7.463	0.6270	−57.71	6.693
20		101	0.8147	−100.4	7.500	0.6271	−57.70	6.722
		161	0.8153	−100.4	7.500	0.6271	−57.70	6.722
	ABAQUS	11,161 (z,x)	0.8140	−100.4	7.520	0.6267	−57.70	6.730
		31,61 (z,x)	0.8124	−100.4	7.101	0.6258	−57.71	6.445
		31,161 (z,x)	0.8147	−100.4	7.560	0.6270	−57.70	6.790
		61,301 (z,x)	0.8152	−100.4	7.489	0.6272	−57.70	6.714

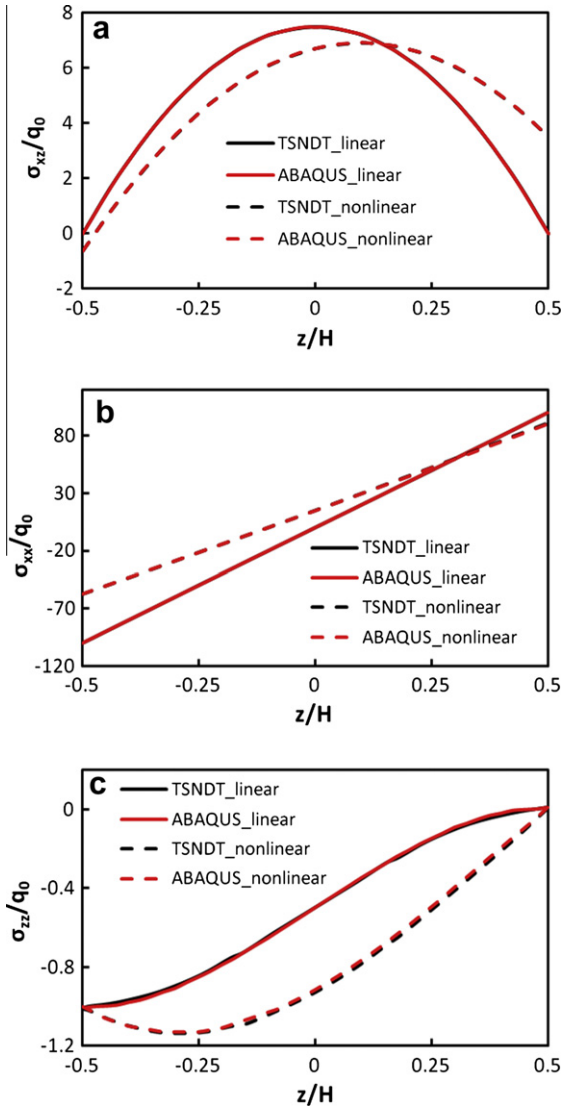

Fig. 9. Comparison of through-the-thickness variations of stresses computed from the linear and the nonlinear theories using the TSNDT and the elasticity (ABAQUS) theories. (a) σ_{xz} at $=\mathcal{L}/4, \mathcal{L}/H = 20, q_0 = 30MPa$; differences in the TSNDT and ABAQUS results from the linear and the nonlinear theories are 0.343% and 0.238%, respectively, and the two sets of results overlap in the Fig. (b) σ_{xx} at $x = \mathcal{L}/2, \mathcal{L}/H = 20, q_0 = 30MPa$; differences in the TSNDT and ABAQUS results from the linear and the nonlinear theories are 0.068% and 0.254%, respectively, and the two sets of results overlap in the Fig. (c) σ_{zz} at $x = \mathcal{L}/2, \mathcal{L}/H = 20, q_0 = 30MPa$; differences in the TSNDT and ABAQUS results from the linear and the nonlinear theories are 1.27% and 1.27%, respectively, and the two sets of results overlap in this figure.

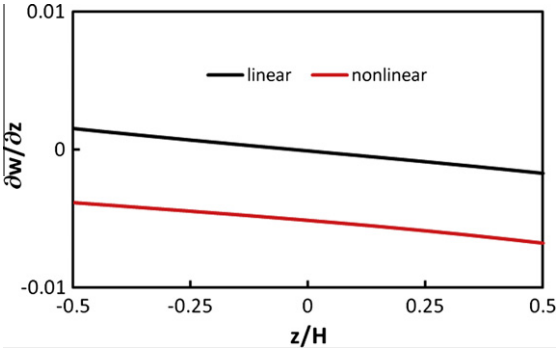

Fig. 10. Variation of $\frac{\partial w}{\partial z}$ through the thickness at $x = \mathcal{L}/4$ for the linear and the nonlinear theories found from the TSNDT solution.

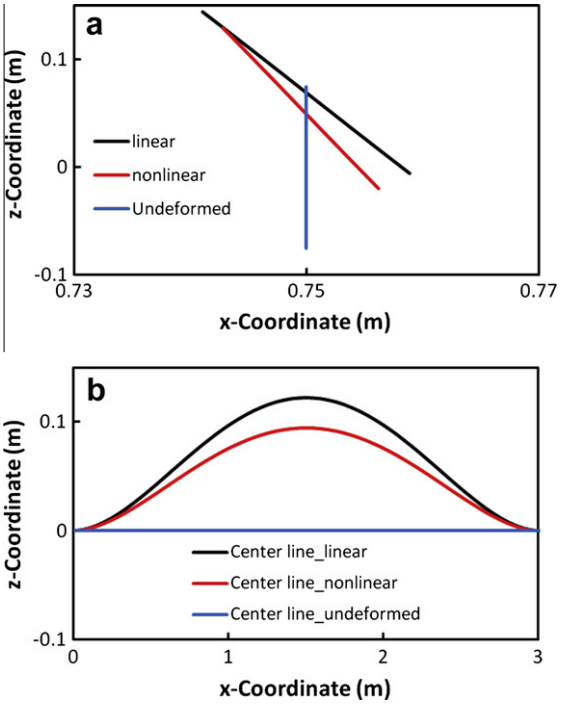

Fig. 11. Deformed and undeformed positions of lines computed using linear and nonlinear theories. (a) Deformed configurations of a line initially perpendicular to the centroidal axis at $x = \mathcal{L}/4$, (b) Deformed shapes of the beam centroidal axis.

Table 8
Non-dimensional deflection, w/H, of the beam centroid with different shape functions, number of nodes along the x-axis, and number of Gauss integration points along the x-axis which are indicated in parentheses.

	21 Nodes	41 Nodes	81 Nodes	Analytical
Linear (1)	0.0321	0.0308	0.0306	0.0303
Linear (3)	0.0287	0.0300	0.0303	
Quadratic (3)	0.0304	0.0304	0.0305	

agreement with the analytical values than those from the HSDST and EHOST that use post-processing methods.

5.2. Finite static deformations of homogeneous straight beam

5.2.1. Comparison of results from the TSNDT with those from ABAQUS

Static finite deformations of clamped–clamped straight 15 cm thick beam with $\mathcal{L}/H = 20$, made of an isotropic and homogeneous St. Venant–Kirchhoff material having E = 172.4 GPa and ν = 0.3 and loaded by a uniform pressure q_0 = 30 MPa on the bottom surface are analyzed as a plane strain problem with ABAQUS and with the TSNDT. We note that the direction of the normal pressure changes as the beam deforms. Values of the centroidal deflection and stresses at critical points from the two approaches and using linear and nonlinear theories are listed in Table 7. For both the linear and the nonlinear theories, converged values of the centroidal deflections and stresses at the point $(\mathcal{L}/4, 0)$ found from the TSNDT and ABAQUS agree well with each other. The computed value of σ_{xx}/q_0 at the point $(\frac{\mathcal{L}}{2}, -\frac{H}{2})$ from the linear theory in which the pressure always acts in the z-direction is nearly twice of that found from the nonlinear theory. The value of $\frac{\sigma_{xz}}{q_0}$ at the point $(\frac{\mathcal{L}}{4}, 0)$ from the linear theory is 11.6% higher than that from the nonlinear theory. *Thus a stress based failure criterion will predict early failure of a material point if stresses from the linear theory are used in it.* Through-the-thickness variations of the axial stress, σ_{xx}, and the transverse stresses, σ_{xz} and σ_{zz}, from the TSNDT and ABAQUS are exhibited in Fig. 9; the percentage differences between the two values of the stress is defined as $100\int_{-H/2}^{H/2}|\sigma_{TSNDT}-\sigma_{ABA}|dz/\int_{-H/2}^{H/2}|\sigma_{ABA}|dz$ where subscripts TSNDT and ABA denote, respectively, values from the TSNDT and ABAQUS solutions. The two values of the percentage difference listed in the figure legends are for results from the linear and the nonlinear theories. With the error of 1.27%, it is clear that stresses computed from the TSNDT and ABAQUS are very close to each other. Whereas σ_{xx} is an affine function of z for both the linear and the nonlinear theories, the values of z where σ_{xx} = 0 are quite different. Through-the-thickness distributions of σ_{zz} from the linear and the nonlinear theories are both qualitatively and quantitatively quite different. Fig. 10 exhibits through-the-thickness variation of $\frac{\partial w}{\partial z}$ at the section $x = \mathcal{L}/4$ found from the linear and the nonlinear theories. Values of $\frac{\partial w}{\partial z}$ are always negative for the nonlinear theory but those from the linear theory are positive at points near the top surface and negative at points near the bottom surface. At a point along the thickness, the magnitude of $\frac{\partial w}{\partial z}$ for the nonlinear theory is more than that from the linear theory. The deformed positions of a line initially perpendicular to the centroidal axis at $x = \mathcal{L}/4$ found from the linear and the nonlinear theories are plotted in Fig. 11. It is evident that the linear and the nonlinear theories give quite different deformed positions of the line.

5.2.2. Verification of the software by the method of manufactured solutions

We use the method of manufactured solutions (e.g., see the material just before and following Eq. (20) of [33]) to verify the code developed for analyzing nonlinear deformations of the beam of Section 5.2.1. For the clamped–clamped beam we begin by assuming the following displacement field

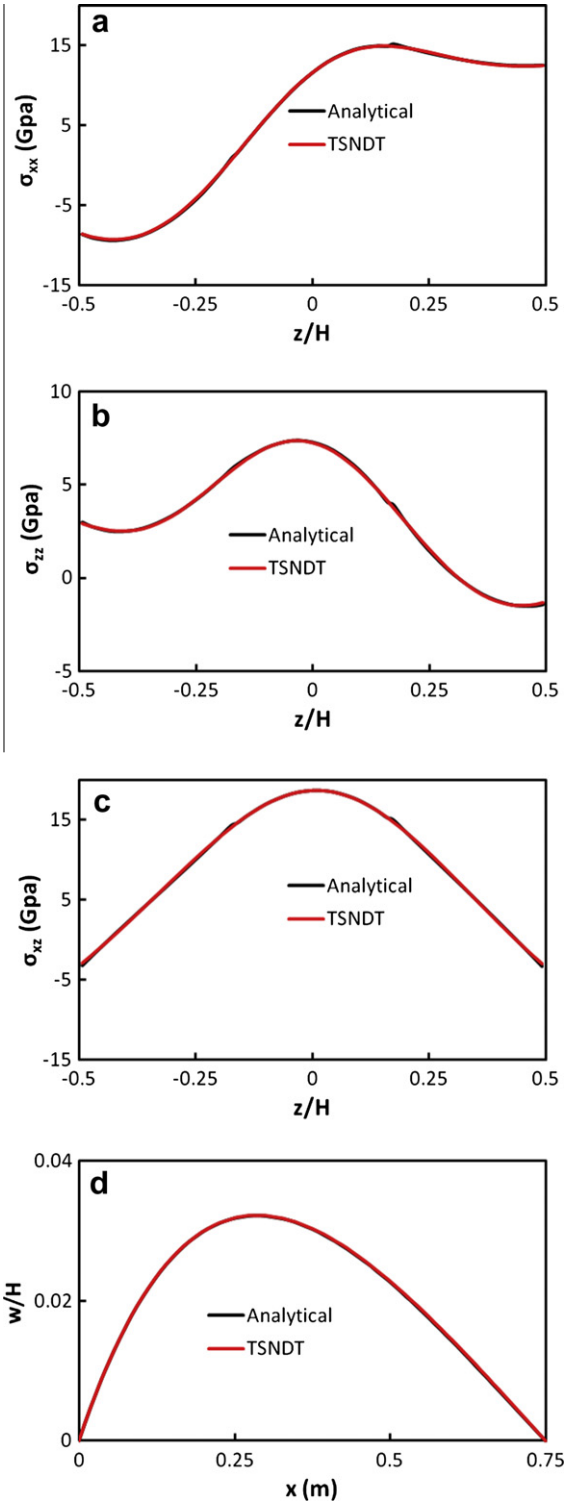

Fig. 12. Comparison of the analytical and the numerical solutions computed using the TSNDT, 81 nodes along the x-axis and piecewise quadratic basis functions. (a) σ_{xx} at x = 0.186 m; difference, $\bar{\eta} = 0.417\%$; the two solutions overlap each other. (b) σ_{zz} at x = 0.186 m; difference, $\bar{\eta} = 0.943\%$; the two solutions overlap each other. (c) σ_{xz} at x = 0.186 m; difference, $\bar{\eta} = 0.715\%$; the two solutions overlap each other. (d) Deflection of the mid-surface, z = 0, of the beam; difference,$\bar{\eta} = 3.33\%$; the two curves overlap each other.

Table 9
Comparison of centroidal deflection and stresses at critical points of curved beam computed by using the TSNDT and ABAQUS.

χ	q_0		Nodes	Linear			Nonlinear		
				w/H $(\mathcal{L}/2,0)$	σ_{xx}/q_0 $(\mathcal{L}/2,H/2)$	σ_{xz}/q_0 $(3\mathcal{L}/4,0)$	w/H $(\mathcal{L}/2,0)$	σ_{xx}/q_0 $(\mathcal{L}/2,H/2)$	σ_{xz}/q_0 $(3\mathcal{L}/4,0)$
		TSNDT	21	0.9080	14.02	−1.144	0.5628	9.845	−1.338
			61	0.9126	14.06	−1.153	0.5622	9.885	−1.346
10	1.38 Gpa		11, 161 (z,x)	0.9128	14.07	−1.114	0.5620	9.885	−1.343
		ABAQUS	31, 161 (z,x)	0.9130	14.07	−1.156	0.5620	9.886	−1.347

$$u = 0.2H\left(\left(\frac{z}{H}\right)^3 + \sin\left(4\frac{z}{H}\right)\right)\left(1-\frac{x}{\mathcal{L}}\right)\frac{x}{\mathcal{L}}e^{\frac{2x}{\mathcal{L}}} \tag{56.a}$$

$$w = 0.2H\left(\left(\frac{z}{H}\right)^4 + \cos\left(2\frac{z}{H}\right)\right)\left(1-\frac{x}{\mathcal{L}}\right)\frac{x}{\mathcal{L}}e^{-\frac{x}{\mathcal{L}}} \tag{56.b}$$

and find strains from Eq. (7) and stresses from Eqs. (23) and (25). Substitution for stresses with acceleration terms set equal to zero in Eq. (12) gives expressions for the body force needed to satisfy equilibrium equations. We find surface tractions on the bounding surfaces from the computed stress field. We now numerically solve the problem with the in-house developed code by using the above found values of the body force and essential boundary conditions applied at both ends of beam and natural boundary conditions on the top and the bottom surfaces of the beam. For the displacement field (56), stress components in Eq. (12) were evaluated numerically by using Eqs. (5), (7), (23) and (25), the spatial derivatives of stresses in Eq. (12) were evaluated by the central difference method, and numerical values of the body force components at each node were read as input into the code.

For $\mathcal{L}/H = 5$ and $\mathcal{L} = 0.75m$, the computed centroidal deflection is compared with its analytical value in Table 8 for piecewise linear and piecewise quadratic basis functions along the x-axis, and using eight integration points in the z-direction in Eq. (28).

It is clear that the converged values of the centroidal deflection are in excellent agreement with the corresponding analytical value. In Fig. 12, the computed through-the-thickness variation of stresses and the deformed shape of the beam are compared with the corresponding ones obtained from the assumed analytical solution. These plots evince that the computed results match well with the corresponding analytical ones.

5.3. Finite static deformations of homogeneous curved beam

The clamped–clamped curved beam studied in subsection 5.1.2 is assumed to be made of an isotropic and homogeneous St. Venant–Kirchhoff material with Young's modulus E = 172 GPa and Poisson's ratio ν = 0.3 and subjected to a sinusoidally varying distributed pressure q_0 on the top surface. The centroidal deflections and stresses at critical points from the TSNDT and ABAQUS solutions listed in Table 9 reveal the following. The centroidal deflection, the axial stress σ_{xx} at $(\mathcal{L}/2, H/2)$, and the transverse shear stress σ_{xz} at $(\mathcal{L}/4, H/2)$ from the linear theory equal 1.624, 1.422 and 0.857 times those from the nonlinear theory. Here $\mathcal{L}$ equals the beam length along the centroidal axis. Through-the-thickness stresses computed from the linear and the nonlinear theories are plotted in Fig. 13. The maximum difference between results from the TSNDT and the ABAQUS is less than 0.8% implying that the TSNDT gives results close to those obtained from the analysis of plane strain deformations of the curved beam using nonlinear elasticity theory. Fig. 14 exhibits through-the-thickness variation of $\frac{\partial w}{\partial z}$ at the section $x = \mathcal{L}/2$.

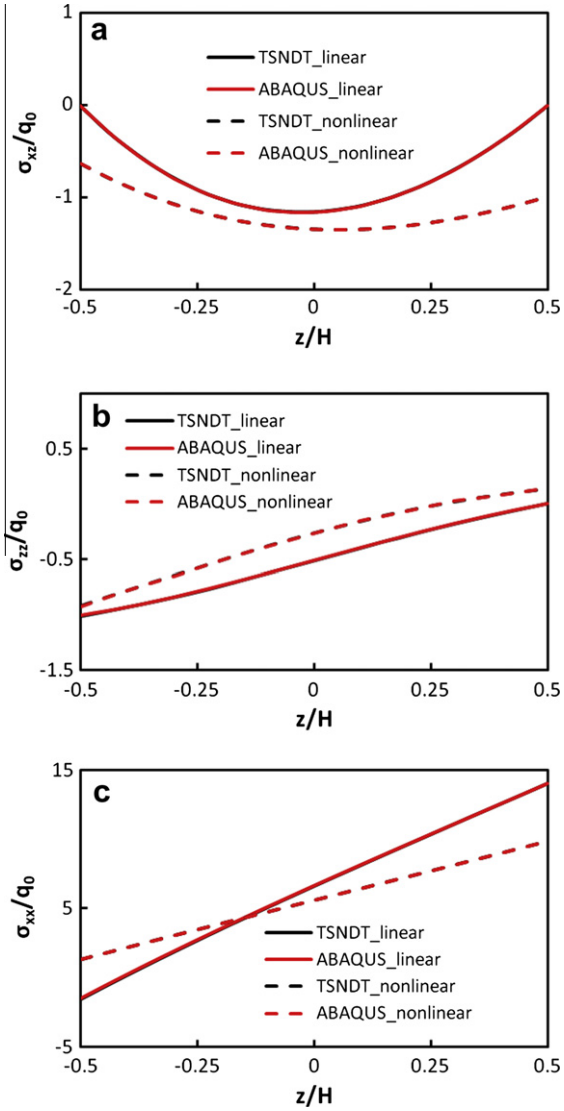

Fig. 13. Comparison of through-the-thickness variation of stresses for the curved beam computed from the linear and the nonlinear theories. (a) σ_{xz} at $x = 3\mathcal{L}/4, \chi = 10, q_0 = 1.38$ GPa ; differences in the TSNDT and the ABAQUS results from the linear and the nonlinear theories are 0.107% and 0.331%, respectively, and results computed using the TSNDT and ABAQUS overlap each other. (b) σ_{zz} at $x = 3\mathcal{L}/4, \chi = 10, q_0 = 1.38$ GPa ; differences in the TSNDT and the ABAQUS results from the linear and the nonlinear theories are 0.279% and 0.706%, respectively, and results computed using the TSNDT and ABAQUS overlap each other. (c) σ_{xx} at $= \mathcal{L}/2, \chi = 10, q_0 = 1.38$ GPa; differences in the TSNDT and the ABAQUS results from the linear and the nonlinear theories are 0.190% and 0.122%, respectively, and the results computed using the TSNDT and ABAQUS overlap each other.

5.4. Transient deformations

5.4.1. Homogeneous straight beam

5.4.1.1. Verification of the software by the method of manufactured solutions. We use the method of manufactured solutions described in subsection 5.2.2 for verifying the in-house developed code for a beam made of a homogeneous and isotropic material and set

$$E = 172.4\,\text{GPa}, \quad \upsilon = 0.3, \quad \rho = 4000\frac{\text{kg}}{\text{m}^3},$$
$$H = 0.15\,\text{m}, \quad \mathcal{L}/H = 20 \tag{57}$$

We assume the following displacement field for a clamped–clamped beam

$$u = 2000H\left(\left(\frac{z}{H}\right)^3 + \sin\left(4\frac{z}{H}\right)\right)\left(1-\frac{x}{\mathcal{L}}\right)\frac{x}{\mathcal{L}}e^{2\frac{x}{L}}(e^t - t - 1.0) \tag{58.a}$$

$$w = 2000H\left(\left(\frac{z}{H}\right)^4 + \cos\left(2\frac{z}{H}\right)\right)\left(1-\frac{x}{\mathcal{L}}\right)\frac{x}{\mathcal{L}}e^{-\frac{x}{L}}(e^t - t - 1.0) \tag{58.b}$$

The procedure outlined in Section 5.2.2 is used to numerically solve the problem. The maximum frequency of the undeformed beam, $\omega_{max} = 1.97 \times 10^6$ rad/s, and the time step used to integrate Eq. (46) is 5.0×10^{-7} s which is less than the critical time step, Δt_{crit}. The time history of the centroidal deflection and through-the-thickness variations of stresses from the numerical and the presumed solutions are shown in Fig. 15. The maximum difference for the centroidal deflection between the TSNDT and the analytical solutions is 3.38% mainly due to the numerical computation of the body forces and inputting those into the code. Through-the-thickness distributions of stresses from the two solutions are very close to each other.

5.4.1.2. Comparison of results from the TSNDT and ABAQUS. For uniformly distributed pressure $q_0 = 20MPa$ applied on the bottom surface of a homogeneous and isotropic straight beam, Fig. 16 shows the time history of the centroidal deflection and deformed positions of the centroidal axis computed using the linear and the nonlinear theories. For each theory, results from the TSNDT and ABAQUS are very close to each other.

5.4.2. Homogeneous curved beam

For the clamped–clamped homogeneous curved beam of Section 5.4 with $\chi = 10$, mass density = 10,684 kg/m^3, and uniformly distributed pressure, $q_0 = 689$ MPa, we have exhibited in Fig. 17 time histories of the centroidal deflection computed using the linear and the nonlinear theories. One can see that results from the TSNDT agree well with those from ABAQUS, and the maximum deflection from the nonlinear theory is considerably less than that from the linear theory. The maximum frequency,ω_{max}, of the beam was found to be 8.43×10^7 rad/s and $\Delta t = 1.5 \times 10^{-8}$ s, which is less than Δt_{crit}, was used to integrate Eq. (46).

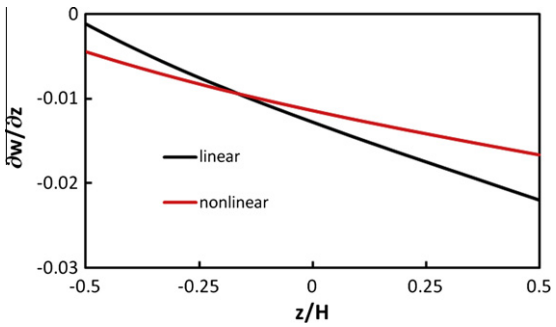

Fig. 14. For the curved beam, variation of $\frac{\partial w}{\partial z}$ through-the-thickness at $x = \mathcal{L}/2$ from the linear and the nonlinear theories.

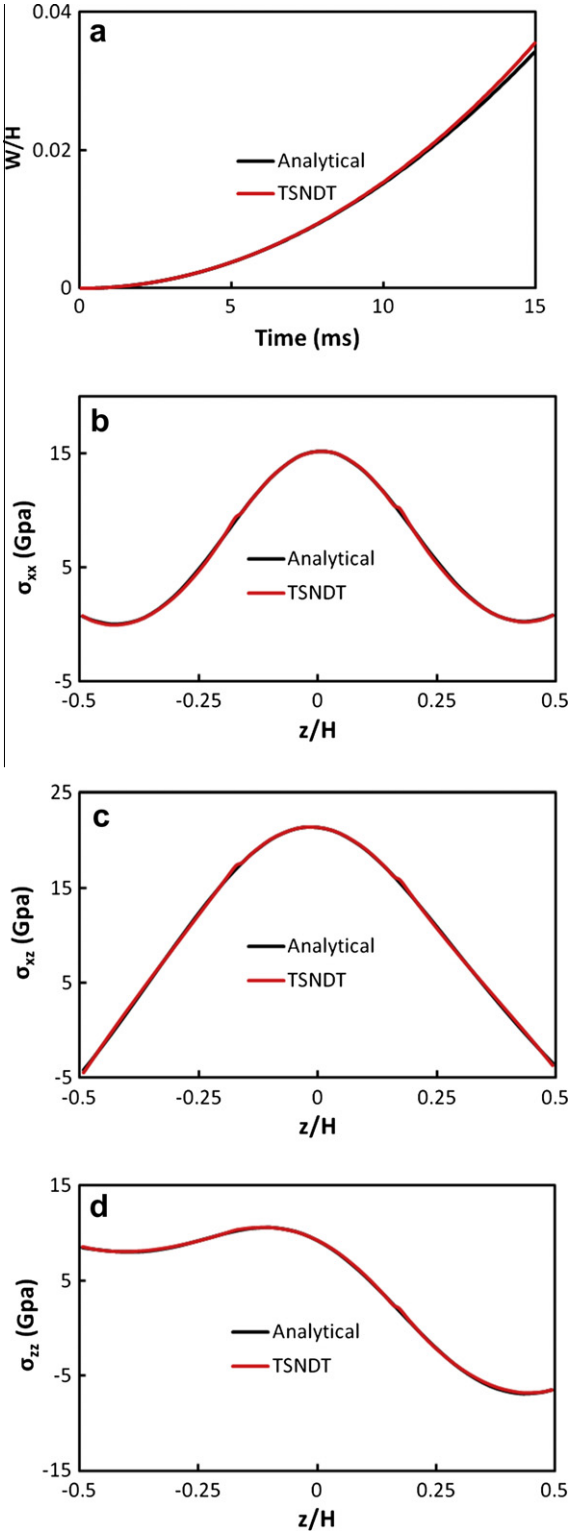

Fig. 15. Comparison of results computed by using the TSNDT with 101 nodes in the x-direction and the analytical solution for the method of manufactured solutions. (a) Time history of deflection at point $(\mathcal{L}/2, 0)$; the difference in the TSNDT and the analytical results from the nonlinear theories is 3.48%, and results from the TSNDT are very close to analytical solution. (b) σ_{xx} at $x = 0.726$ m when $t = 15$ ms; the difference in the TSNDT and the analytical results from the nonlinear theories equals 0.7%, and results from the TSNDT are very close to analytical solution. (c) σ_{xz} at $x = 0.726$ m when $t = 15$ ms; the difference in the TSNDT and the analytical results from the nonlinear theories equals 0.65%, and results from the TSNDT are very close to analytical solution. (d) σ_{zz} at $x = 0.726$ m when $t = 15$ ms; the difference in the TSNDT and the analytical results from the nonlinear theories equals 0.25%, and results from the TSNDT are very close to analytical solution.

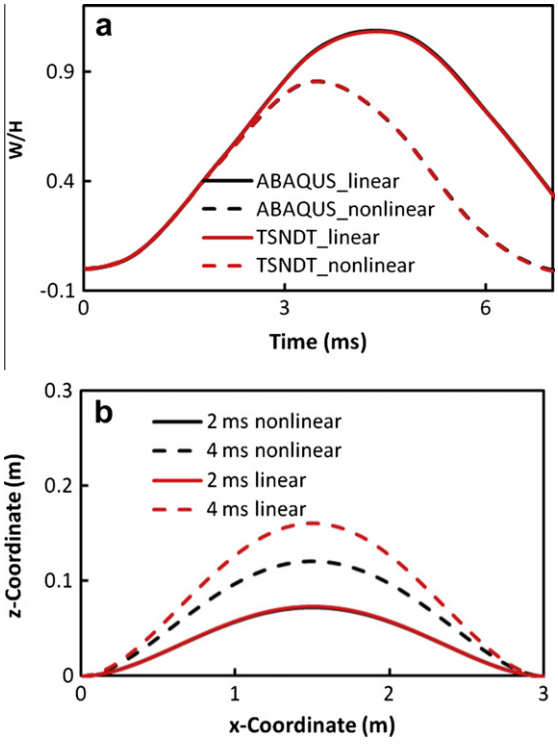

Fig. 16. Comparison of results computed by using the TSNDT and ABAQUS with and without considering geometric nonlinearities. (a) Time histories of the centroidal deflection from the linear and the nonlinear theories; for each theory results from the TSNDT and ABAQUS essentially overlap each other. (b) Deformed positions of the centroidal axis at $t = 2$ and 4 ms from the linear and the nonlinear theories computed using the TSNDT.

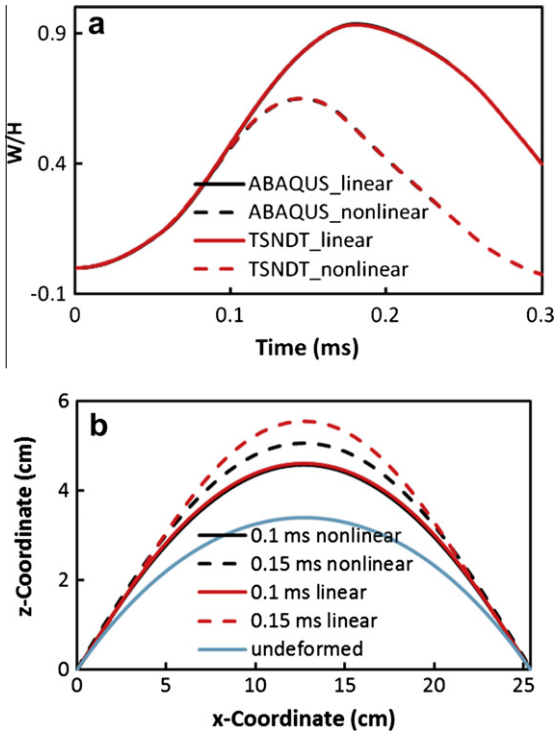

Fig. 17. Comparison of results computed by using the TSNDT (61 nodes) and ABAQUS with and without considering geometric nonlinearities. (a) Time histories of the deflection of the beam centroid from the linear and the nonlinear theories; for each theory results from the TSNDT and ABAQUS essentially overlap each other. (b) Deformed positions of the centroidal axis at $t = 0.1$ and 0.15 ms from the linear and the nonlinear theories computed using the TSNDT (x and z are global coordinate in this plot).

6. Conclusions

A third order shear and normal deformable beam theory (TSNDT) for analyzing finite deformations of a curved laminated beam made of a St. Venant–Kirchhoff material has been developed. It has been used in combination with the finite element method (FEM) to analyze static and dynamic deformations of straight and curved beams by considering all geometric nonlinear effects. Equations governing deformations of the beam are written in the Lagrangian description of motion using continuum mechanics principles, and a weak form of the governing equations has been derived. No shear correction factor is used, and stresses are derived from the displacement field and the constitutive relation without using any post-processing technique. The method of manufactured solutions has been used to verify the in-house developed software capable of analyzing static and dynamic problems. Furthermore, for both straight and curved beams, deflections and stresses computed using the TSNDT for linear and nonlinear theories agree very well with those obtained using the commercial FE software ABAQUS that analyzes plane strain deformations of the beam modeled as a continuum. For a curved beam made of a homogeneous and isotropic material and radius of curvature/beam thickness = 10, it is found that the maximum transverse deflections and axial stresses at critical points computed using the linear theory are nearly 60% and 40% more than those obtained from the nonlinear theory. However, the transverse shear stresses from the linear theory equal about 86% of those from the nonlinear theory. Thus a stress based failure criterion will predict premature failure of the beam if stresses are derived from the linear elasticity theory.

Acknowledgements

This work was supported by the Office of Naval Research Grant N00014-11-1-0594 to Virginia Polytechnic Institute and State University with Dr. Y.D.S. Rajapakse as the Program Manager. Views expressed in the paper are those of the authors and neither of the funding agency nor of authors' Institution.

Appendix A

Expressions of non-zero terms of M^j_{mn} are listed below.

$$M^j_{11} = C^{1jb}_{1111}e^b_{11} + C^{1jb}_{1133}e^b_{33} + C^{3jbd}_{1111}\frac{1}{2}\eta^{bd}_{11} + C^{3jbd}_{1133}\frac{1}{2}\eta^{bd}_{33} + C^{4jib}_{1111}e^i_{11}e^b_{11} + C^{4jib}_{1133}e^i_{11}e^b_{33} + C^{4jib}_{3113}e^i_{13}e^b_{13} + C^{4jib}_{3131}e^i_{13}e^b_{31} + C^{6jibd}_{1111}\frac{1}{2}e^i_{11}\eta^{bd}_{11} + C^{6jibd}_{1133}\frac{1}{2}e^i_{11}\eta^{bd}_{33} + C^{6jibd}_{3113}e^i_{13}\eta^{bd}_{13}$$

$$M^j_{33} = C^{1jb}_{3311}e^b_{11} + C^{1jb}_{3333}e^b_{33} + C^{3jbd}_{3311}\frac{1}{2}\eta^{bd}_{11} + C^{3jbd}_{3333}\frac{1}{2}\eta^{bd}_{33} + C^{4jib}_{3311}e^i_{33}e^b_{11} + C^{4jib}_{3333}e^i_{33}e^b_{33} + C^{4jib}_{1313}e^i_{31}e^b_{13} + C^{4jib}_{1331}e^i_{31}e^b_{31} + C^{6jibd}_{3311}\frac{1}{2}e^i_{33}\eta^{bd}_{11} + C^{6jibd}_{3333}\frac{1}{2}e^i_{33}\eta^{bd}_{33} + C^{6jibd}_{1313}e^i_{31}\eta^{bd}_{13}$$

$$M^j_{13} = C^{1jb}_{1313}e^b_{13} + C^{1jb}_{1331}e^b_{31} + C^{3jbd}_{1313}\eta^{bd}_{13} + C^{4jib}_{3311}e^i_{13}e^b_{11} + C^{4jib}_{3333}e^i_{13}e^b_{33} + C^{4jib}_{1331}e^i_{11}e^b_{31} + C^{4jib}_{1313}e^i_{11}e^b_{13} + C^{6jibd}_{3311}\frac{1}{2}e^i_{13}\eta^{bd}_{11} + C^{6jibd}_{3333}\frac{1}{2}e^i_{13}\eta^{bd}_{33} + C^{6jibd}_{1313}e^i_{11}\eta^{bd}_{13}$$

$$M^j_{31} = C^{1jb}_{3113}e^b_{13} + C^{1jb}_{3131}e^b_{31} + C^{3jbd}_{3113}\eta^{bd}_{13} + C^{4jib}_{1111}e^i_{31}e^b_{11} + C^{4jib}_{1133}e^i_{31}e^b_{33} + C^{4jib}_{3131}e^i_{33}e^b_{31} + C^{4jib}_{3113}e^i_{33}e^b_{13} + C^{6jibd}_{1111} \times \frac{1}{2}e^i_{31}\eta^{bd}_{11} + C^{6jibd}_{1133}\frac{1}{2}e^i_{31}\eta^{bd}_{33} + C^{6jibd}_{3113}e^i_{33}\eta^{bd}_{13} \quad (A.1)$$

Here $i, j, b, d = 0, 1, 2, 3$

For the beam made of an isotropic material with Young's modulus E and Poisson's ratio υ, we set

$$\mu_0 = \frac{E(1-\upsilon)}{(1-2\upsilon)(1+\upsilon)}, \quad \mu_1 = \frac{E\upsilon}{(1-2\upsilon)(1+\upsilon)}, \quad \mu_2 = \frac{E1}{2(1+\upsilon)} \quad (A.2)$$

When the beam is either straight or the curved beam is thin enough to neglect through-the-thickness variation of H_1, Eq. (A.1) are simplified into Eq. (A.3).

$$\chi^{\mathrm{ibd}}_{33} = \mu_1\frac{1}{2}e^i_{33}\eta^{bd}_{11} + \frac{1}{2}\mu_0 e^i_{33}\eta^{bd}_{33} + \mu_2 e^i_{31}\eta^{bd}_{13}$$
$$\chi^{\mathrm{ibd}}_{13} = \mu_1\frac{1}{2}e^i_{13}\eta^{bd}_{11} + \frac{1}{2}\mu_0 e^i_{13}\eta^{bd}_{33} + \mu_2 e^i_{11}\eta^{bd}_{13}$$
$$\chi^{\mathrm{ibd}}_{31} = \mu_0\frac{1}{2}e^i_{31}\eta^{bd}_{11} + \mu_1\frac{1}{2}e^i_{31}\eta^{bd}_{33} + \mu_2 e^i_{33}\eta^{bd}_{13} \quad (A.6)$$

where $\chi_{\mathrm{mn}}{}^{\mathrm{ibd}} = \chi_{\mathrm{mn}}{}^{\mathrm{idb}}$, $m, n = 1, 3$.

Thus constitutive equations (A.3) for the FSNDT become

$$M^0_{mn} = I^0(\epsilon^0_{mn} + \Upsilon^{00}_{\mathrm{mn}} + \chi^{000}_{\mathrm{mn}}) + I^2(\Upsilon^{11}_{\mathrm{mn}} + +\chi^{011}_{\mathrm{mn}} + 2\chi^{101}_{\mathrm{mn}})$$
$$M^1_{mn} = I^2(\epsilon^1_{mn} + \Upsilon^{01}_{\mathrm{mn}} + \Upsilon^{10}_{\mathrm{mn}} + \chi^{100}_{\mathrm{mn}} + 2\chi^{010}_{\mathrm{mn}}) + I^4\chi^{111}_{\mathrm{mn}} \quad (A.7)$$

where indices $m, n = 1, 3$, and those for the TSNDT can be simplified into the following expressions.

$$M^j_{11} = C^{2jb}(\mu_0 e^b_{11} + \mu_1 e^b_{33}) + C^{3jbd}\left(\frac{1}{2}\mu_0\eta^{bd}_{11} + \frac{1}{2}\mu_1\eta^{bd}_{33} + \mu_0 e^b_{11}e^d_{11} + \mu_1 e^b_{11}e^d_{33} + \mu_2 e^b_{13}e^d_{13} + \mu_2 e^b_{13}e^d_{31}\right) + C^{4jibd}\left(\frac{1}{2}\mu_0 e^i_{11}\eta^{bd}_{11} + \mu_1\frac{1}{2}e^i_{11}\eta^{bd}_{33} + \mu_2 e^i_{13}\eta^{bd}_{13}\right)$$
$$M^j_{33} = C^{2jb}(\mu_1 e^b_{11} + \mu_0 e^b_{33}) + C^{3jbd}\left(\mu_1\frac{1}{2}\eta^{bd}_{11} + \mu_0\frac{1}{2}\eta^{bd}_{33} + \mu_1 e^b_{33}e^d_{11} + \mu_0 e^b_{33}e^d_{33} + \mu_2 e^b_{31}e^d_{13} + \mu_2 e^b_{31}e^d_{31}\right) + C^{4jibd}\left(\mu_1\frac{1}{2}e^i_{33}\eta^{bd}_{11} + \frac{1}{2}\mu_0 e^i_{33}\eta^{bd}_{33} + \mu_2 e^i_{31}\eta^{bd}_{13}\right)$$
$$M^j_{13} = C^{2jb}\mu_2(e^b_{13} + e^b_{31}) + C^{3jbd}(\mu_2\eta^{bd}_{13} + \mu_1 e^b_{13}e^d_{11} + \mu_0 e^b_{13}e^d_{33} + \mu_2 e^b_{11}e^d_{31} + \mu_2 e^b_{11}e^d_{13}) + C^{4jibd}\left(\mu_1\frac{1}{2}e^i_{13}\eta^{bd}_{11} + \frac{1}{2}\mu_0 e^i_{13}\eta^{bd}_{33} + \mu_2 e^i_{11}\eta^{bd}_{13}\right)$$
$$M^j_{31} = C^{2jb}\mu_2(e^b_{13} + e^b_{31}) + C^{3jbd}(\mu_2\eta^{bd}_{13} + \mu_0 e^b_{31}e^d_{11} + \mu_1 e^b_{31}e^d_{33} + \mu_2 e^b_{33}e^d_{31} + \mu_2 e^b_{33}e^d_{13}) + C^{4jibd}\left(\mu_0\frac{1}{2}e^i_{31}\eta^{bd}_{11} + \mu_1\frac{1}{2}e^i_{31}\eta^{bd}_{33} + \mu_2 e^i_{33}\eta^{bd}_{13}\right) \quad (A.3)$$

where

$$C^{2jb} = \int_{-\mathrm{H}/2}^{\mathrm{H}/2} L_j L_b dy_3 = I^{j+b}$$
$$C^{3jbd} = \int_{-\mathrm{H}/2}^{\mathrm{H}/2} L_j L_b L_d dy_3 = I^{j+b+d}$$
$$C^{4jibd} = \int_{-\mathrm{H}/2}^{\mathrm{H}/2} L_j L_i L_b L_d dy_3 = I^{j+i+b+d}$$
$$I^\theta = \int_{-\mathrm{H}/2}^{\mathrm{H}/2} z^\theta dy_3, \quad \theta = 0, 1, \cdots 12 \quad (A.4)$$

The seven non-zero terms of I^θ are

$$I^0 = \mathrm{H}, \quad I^2 = \frac{\mathrm{H}^3}{12}, \quad I^4 = \frac{\mathrm{H}^5}{80}, \quad I^6 = \frac{\mathrm{H}^7}{448}, \quad I^8 = \frac{\mathrm{H}^9}{2304}, \quad I^{10} = \frac{\mathrm{H}^{11}}{11,264}, \quad I^{12} = \frac{\mathrm{H}^{13}}{53,248} \quad (A.5)$$

In order to explicitly write constitutive equations (A.3) for the first order shear and normal deformable plate theory (FSNDT) for a thin shell made of an isotropic and homogeneous material, we set

$$\epsilon^b_{11} = \mu_0 e^b_{11} + \mu_1 e^b_{33}, \quad \epsilon^b_{33} = \mu_1 e^b_{11} + \mu_0 e^b_{33}, \quad \epsilon^b_{13} = \epsilon^b_{31} = \mu_2(e^b_{13} + e^b_{31})$$
$$\Upsilon^{\mathrm{bd}}_{11} = \frac{1}{2}\mu_0\eta^{bd}_{11} + \frac{1}{2}\mu_1\eta^{bd}_{33} + \mu_0 e^b_{11}e^d_{11} + \mu_1 e^b_{11}e^d_{33} + \mu_2 e^b_{13}e^d_{13} + \mu_2 e^b_{13}e^d_{31}$$
$$\Upsilon^{\mathrm{bd}}_{33} = \mu_1\frac{1}{2}\eta^{bd}_{11} + \frac{1}{2}\mu_0\eta^{bd}_{33} + \mu_1 e^b_{33}e^d_{11} + \mu_0 e^b_{33}e^d_{33} + \mu_2 e^b_{31}e^d_{13} + \mu_2 e^b_{31}e^d_{31}$$
$$\Upsilon^{\mathrm{bd}}_{13} = \mu_2\eta^{bd}_{13} + \mu_1 e^b_{13}e^d_{11} + \mu_0 e^b_{13}e^d_{33} + \mu_2 e^b_{11}e^d_{31} + \mu_2 e^b_{11}e^d_{13}$$
$$\Upsilon^{\mathrm{bd}}_{31} = \mu_2\eta^{bd}_{13} + \mu_0 e^b_{31}e^d_{11} + \mu_1 e^b_{31}e^d_{33} + \mu_2 e^b_{33}e^d_{31} + \mu_2 e^b_{33}e^d_{13}$$
$$\chi^{\mathrm{ibd}}_{11} = \mu_0\frac{1}{2}e^i_{11}\eta^{bd}_{11} + \mu_1\frac{1}{2}e^i_{11}\eta^{bd}_{33} + \mu_2 e^i_{13}\eta^{bd}_{13}$$

$$M^0_{mn} = I^0(\epsilon^0_{mn} + \Upsilon^{00}_{\mathrm{mn}} + \chi^{000}_{\mathrm{mn}}) + I^2(\epsilon^2_{mn} + \Upsilon^{11}_{\mathrm{mn}} + \Upsilon^{20}_{\mathrm{mn}} + \Upsilon^{02}_{\mathrm{mn}} + 2\chi^{002}_{\mathrm{mn}} + \chi^{011}_{\mathrm{mn}} + 2\chi^{101}_{\mathrm{mn}}\chi^{200}_{\mathrm{mn}}) + I^4(\Upsilon^{13}_{\mathrm{mn}} + \Upsilon^{31}_{\mathrm{mn}} + \Upsilon^{22}_{\mathrm{mn}} + \chi^{022}_{\mathrm{mn}} + 2\chi^{031}_{\mathrm{mn}} + 2\chi^{130}_{\mathrm{mn}} + 2\chi^{121}_{\mathrm{mn}} + 2\chi^{220}_{\mathrm{mn}} + \chi^{211}_{\mathrm{mn}} + 2\chi^{310}_{\mathrm{mn}}) + I^6(\chi^{33}_{\mathrm{mn}} + \chi^{033}_{\mathrm{mn}} + 2\chi^{123}_{\mathrm{mn}} + \chi^{222}_{\mathrm{mn}} + 2\chi^{231}_{\mathrm{mn}} + 2\chi^{303}_{\mathrm{mn}}) + I^8(2\chi^{323}_{\mathrm{mn}} + \chi^{233}_{\mathrm{mn}})$$
$$M^1_{mn} = I^2(\epsilon^1_{mn} + \Upsilon^{01}_{\mathrm{mn}} + \Upsilon^{10}_{\mathrm{mn}} + \chi^{100}_{\mathrm{mn}} + 2\chi^{010}_{\mathrm{mn}}) + I^4(\epsilon^3_{mn} + \Upsilon^{21}_{\mathrm{mn}} + \Upsilon^{12}_{\mathrm{mn}} + \Upsilon^{30}_{\mathrm{mn}} + \Upsilon^{03}_{\mathrm{mn}} + \chi^{300}_{\mathrm{mn}} + 2\chi^{030}_{\mathrm{mn}} + 2\chi^{021}_{\mathrm{mn}} + 2\chi^{120}_{\mathrm{mn}} + \chi^{111}_{\mathrm{mn}} + 2\chi^{210}_{\mathrm{mn}}) + I^6(\Upsilon^{23}_{\mathrm{mn}} + \Upsilon^{32}_{\mathrm{mn}} + 2\chi^{320}_{\mathrm{mn}} + \chi^{311}_{\mathrm{mn}} + 2\chi^{230}_{\mathrm{mn}} + 2\chi^{212}_{\mathrm{mn}} + 2\chi^{131}_{\mathrm{mn}} + \chi^{122}_{\mathrm{mn}} + 2\chi^{023}_{\mathrm{mn}}) + I^8(2\chi^{313}_{\mathrm{mn}} + \chi^{322}_{\mathrm{mn}} + 2\chi^{232}_{\mathrm{mn}} + \chi^{133}_{\mathrm{mn}})$$
$$M^2_{mn} = I^2(\epsilon^0_{mn} + \Upsilon^{00}_{\mathrm{mn}} + \chi^{000}_{\mathrm{mn}}) + I^4(\epsilon^2_{mn} + \Upsilon^{11}_{\mathrm{mn}} + \Upsilon^{20}_{\mathrm{mn}} + \Upsilon^{02}_{\mathrm{mn}} + 2\chi^{002}_{\mathrm{mn}} + \chi^{011}_{\mathrm{mn}} + 2\chi^{101}_{\mathrm{mn}}\chi^{200}_{\mathrm{mn}}) + I^6(\Upsilon^{13}_{\mathrm{mn}} + \Upsilon^{31}_{\mathrm{mn}} + \Upsilon^{22}_{\mathrm{mn}} + \chi^{022}_{\mathrm{mn}} + 2\chi^{031}_{\mathrm{mn}} + 2\chi^{130}_{\mathrm{mn}} + 2\chi^{121}_{\mathrm{mn}} + 2\chi^{220}_{\mathrm{mn}} + \chi^{211}_{\mathrm{mn}} + 2\chi^{310}_{\mathrm{mn}}) + I^8(\chi^{33}_{\mathrm{mn}} + \chi^{033}_{\mathrm{mn}} + 2\chi^{123}_{\mathrm{mn}} + \chi^{222}_{\mathrm{mn}} + 2\chi^{231}_{\mathrm{mn}} + 2\chi^{303}_{\mathrm{mn}}) + I^{10}(2\chi^{323}_{\mathrm{mn}} + \chi^{233}_{\mathrm{mn}})$$
$$M^3_{mn} = I^4(\epsilon^1_{mn} + \Upsilon^{01}_{\mathrm{mn}} + \Upsilon^{10}_{\mathrm{mn}} + \chi^{100}_{\mathrm{mn}} + 2\chi^{010}_{\mathrm{mn}}) + I^6(\epsilon^3_{mn} + \Upsilon^{21}_{\mathrm{mn}} + \Upsilon^{12}_{\mathrm{mn}} + \Upsilon^{30}_{\mathrm{mn}} + \Upsilon^{03}_{\mathrm{mn}} + \chi^{300}_{\mathrm{mn}} + 2\chi^{030}_{\mathrm{mn}} + 2\chi^{021}_{\mathrm{mn}} + 2\chi^{120}_{\mathrm{mn}} + \chi^{111}_{\mathrm{mn}} + 2\chi^{210}_{\mathrm{mn}}) + I^8(\Upsilon^{23}_{\mathrm{mn}} + \Upsilon^{32}_{\mathrm{mn}} + 2\chi^{320}_{\mathrm{mn}} + \chi^{311}_{\mathrm{mn}} + 2\chi^{230}_{\mathrm{mn}} + 2\chi^{212}_{\mathrm{mn}} + 2\chi^{131}_{\mathrm{mn}} + \chi^{122}_{\mathrm{mn}} + 2\chi^{023}_{\mathrm{mn}}) + I^{10}(2\chi^{313}_{\mathrm{mn}} + \chi^{322}_{\mathrm{mn}} + 2\chi^{232}_{\mathrm{mn}} + \chi^{133}_{\mathrm{mn}}) + I^{12}\chi^{333}_{\mathrm{mn}} \quad (A.8)$$

where $m, n = 1, 3$.

Appendix B

Expressions of components of $[\kappa]$ are listed below.

$$k_{11}^{jb} = C_{1111}^{1jb} + C_{1111}^{3jib} e_{11}^{i} + 2C_{1111}^{4jib} e_{11}^{i} + C_{1133}^{4jib} e_{33}^{i} + C_{1111}^{6jbid} \frac{1}{2} \eta_{11}^{id} + C_{1111}^{6jibd} e_{11}^{i} e_{11}^{d} C_{1133}^{6jbid} \frac{1}{2} \eta_{33}^{id} + C_{3113}^{6jibd} e_{13}^{i} e_{13}^{d}$$

$$k_{12}^{jb} = C_{1133}^{1jb} + C_{1133}^{3jib} e_{33}^{i} + C_{1133}^{4jib} e_{11}^{i} + C_{1133}^{6jibd} e_{11}^{i} e_{33}^{d} + C_{3113}^{6jibd} e_{13}^{i} e_{31}^{d}$$

$$k_{13}^{jb} = C_{1133}^{3jib} e_{13}^{i} + 2C_{3113}^{4jib} e_{13}^{i} + C_{3131}^{4jib} e_{31}^{i} + C_{1133}^{6jibd} e_{11}^{i} e_{13}^{d} + C_{3113}^{6jbid} \eta_{13}^{id} + C_{3113}^{6jibd} e_{13}^{i} e_{11}^{d}$$

$$k_{14}^{jb} = C_{1111}^{3jib} e_{31}^{i} + C_{3131}^{4jib} e_{13}^{i} + C_{1111}^{6jibd} \frac{1}{2} e_{11}^{i} e_{31}^{d} + C_{3113}^{6jibd} e_{13}^{i} e_{33}^{b}$$

$$\kappa_{21}^{jb} = C_{3311}^{1jb} + C_{3311}^{3jbd} e_{11}^{d} + C_{3311}^{4jib} e_{33}^{i} + C_{3311}^{6jibd} e_{33}^{i} e_{11}^{d} + C_{1313}^{6jibd} e_{31}^{i} e_{13}^{d}$$

$$\kappa_{22}^{jb} = C_{3333}^{1jb} + C_{3333}^{3jbd} e_{33}^{d} + C_{3311}^{4jbi} e_{11}^{i} + 2C_{3333}^{4jib} e_{33}^{i} + C_{3311}^{6jibd} \frac{1}{2} \eta_{11}^{bd} + C_{3333}^{6jbid} \frac{1}{2} \eta_{33}^{bd} + C_{3333}^{6jibd} e_{33}^{i} e_{33}^{d} + C_{1313}^{6jibd} e_{31}^{i} e_{31}^{d}$$

$$\kappa_{23}^{jb} = C_{3333}^{3jbd} e_{13}^{d} + C_{1313}^{4jib} e_{31}^{i} + 2C_{1331}^{4jib} e_{31}^{i} + C_{3333}^{6jibd} e_{33}^{i} e_{33}^{d} + C_{1313}^{6jibd} e_{31}^{i} e_{11}^{d}$$

$$\kappa_{24}^{jb} = C_{3311}^{3jbd} e_{31}^{d} + C_{1313}^{4jbi} e_{13}^{i} + C_{3311}^{6jibd} e_{33}^{i} e_{31}^{d} + C_{1313}^{6jibd} \eta_{13}^{id} + C_{1313}^{6jibd} e_{31}^{i} e_{33}^{d}$$

$$\kappa_{31}^{jb} = C_{1313}^{3jbd} e_{13}^{d} + C_{3311}^{4jib} e_{13}^{i} + C_{1331}^{4jbi} e_{31}^{i} + C_{1313}^{4jbi} e_{13}^{i} + C_{3311}^{6jibd} e_{13}^{i} e_{11}^{d} + C_{1313}^{6jbid} \eta_{13}^{id} + C_{1313}^{6jibd} e_{11}^{i} e_{13}^{d}$$

$$\kappa_{32}^{jb} = C_{1313}^{3jdb} e_{31}^{d} + C_{3333}^{4jib} e_{13}^{i} + C_{3333}^{6jibd} e_{13}^{i} e_{33}^{d} + C_{1313}^{6jibd} e_{11}^{i} e_{31}^{d}$$

$$\kappa_{33}^{jb} = C_{1313}^{1jb} + C_{1313}^{3jdb} e_{11}^{d} + C_{3311}^{4jbi} e_{11}^{i} + C_{3333}^{4jbi} e_{33}^{i} + C_{1313}^{4jib} e_{11}^{i} + C_{3311}^{6jbid} \frac{1}{2} \eta_{11}^{id} + C_{3333}^{6jbid} \frac{1}{2} \eta_{33}^{id} + C_{3333}^{6jibd} e_{13}^{i} e_{13}^{d} + C_{1313}^{6jibd} e_{11}^{i} e_{11}^{d}$$

$$\kappa_{34}^{jb} = C_{1331}^{1jb} + C_{1313}^{3jbd} e_{33}^{d} + C_{1331}^{4jib} e_{11}^{i} + C_{3311}^{6jibd} e_{13}^{i} e_{31}^{d} + C_{1313}^{6jibd} e_{11}^{i} e_{33}^{d}$$

$$\kappa_{41}^{jb} = C_{3113}^{3jbd} e_{13}^{d} + C_{1111}^{4jib} e_{31}^{i} + C_{1111}^{6jibd} e_{31}^{i} e_{11}^{d} + C_{3113}^{6jibd} \frac{1}{2} e_{33}^{i} e_{13}^{d}$$

$$\kappa_{42}^{jb} = C_{3113}^{3jbd} e_{31}^{d} + C_{1133}^{4jib} e_{31}^{i} + C_{3131}^{4jbi} e_{31}^{i} + C_{3113}^{4jib} e_{13}^{i} + C_{1133}^{6jibd} e_{31}^{i} e_{33}^{d} + C_{3113}^{6jbid} \frac{1}{2} \eta_{13}^{id} + C_{3113}^{6jibd} \frac{1}{2} e_{33}^{i} e_{31}^{d}$$

$$\kappa_{43}^{jb} = C_{3113}^{1jb} + C_{3113}^{3jdb} e_{11}^{d} + C_{3113}^{4jib} e_{33}^{i} + C_{1111}^{6jibd} e_{31}^{i} e_{31}^{d} + C_{1133}^{6jibd} e_{31}^{i} e_{13}^{d} + C_{3113}^{6jibd} \frac{1}{2} e_{33}^{i} e_{11}^{d}$$

$$\kappa_{44}^{jb} = C_{3131}^{1jb} + C_{3113}^{3jbd} e_{33}^{d} + C_{1111}^{4jbi} e_{11}^{i} + C_{1133}^{4jbi} e_{33}^{i} + C_{3131}^{4jib} e_{33}^{i} + C_{1111}^{6jbid} \frac{1}{2} \eta_{11}^{id} + C_{1133}^{6jbid} \frac{1}{2} \eta_{33}^{id} + C_{3113}^{6jibd} \frac{1}{2} e_{33}^{i} e_{33}^{d}$$

Here $i, j, b, d = 0, 1, 2, 3$.

References

[1] Carrera E. Historical review of zig–zag theories for multilayered plates and shells. Appl Mech Rev 2003;56(3):287–308.
[2] Reddy JN, Arciniega RA. Shear deformation plate and shell theories: from Stavsky to present. Mech Advan Mater Struct 2004;11(6):535–82.
[3] Kant T, Swaminathan K. Estimation of transverse/interlaminar stresses in laminated composites – a selective review and survey of current developments. Compos Struct 2000;49(1):65–75.
[4] Reissner E. The effect of transverse shear deformation on the bending of elastic plates. J Appl Mech 1945;12(2):69–77.
[5] Mindlin RD. Influence of rotatory inertia and shear on flexural motions of isotropic, elastic plates. J Appl Mech 1951;18(1):31–8.
[6] Reddy JN, Liu CF. A higher-order shear deformation theory of laminated elastic shells. Int J Eng Sci 1985;23(3):319–30.
[7] Lekhnitskii SG. Strength calculation of composite beams. Vestnik inzhen i tekhnikov 1935;9.
[8] Ren JG. A new theory of laminated plate. Compos Sci Technol 1986; 26(3):225–39.
[9] Ren JG. Bending theory of laminated plate. Compos Sci Technol 1986; 27(3):225–48.
[10] Ren JG, Owen DRJ. Vibration and buckling of laminated plates. Int J Solids Struct 1989;25(2):95–106.
[11] Ambartsumyan SA. Theory of anisotropic shells; 1964.
[12] Whitney JM. The effect of transverse shear deformation on the bending of laminated plates. J Compos Mater 1969;3(3):534–47.
[13] Reissner E. On a mixed variational theorem and on shear deformable plate theory. Int J Numer Meth Eng 1986;23(2):193–8.
[14] Koiter WT. A consistent first approximation in the general theory of thin elastic shells; 1960.
[15] Rybov AF. Fundamental equations of the theory of multilayered shells taking account of transverse shear strain. In: Strength of materials and theory of structures, vol. 3. Budivelnik, Kiev, 1964.
[16] Rybov AF. On the theory multilayered shell shells with filler. In: Air force construction and air force Engineering, vol. 11. Izd Khakosvsk, Univ, Kharkov, 1967.
[17] Rasskazov AO. Theory of multilayer orthotropic shallow shells. Int Appl Mech 1976;12(11):1131–6.
[18] Carrera E, Antona E. A class of two-dimensional theories for anisotropic multilayered plates analysis. Accademia delle Scienze; 1995.
[19] Carrera E. Mixed layer-wise models for multilayered plates analysis. Compos Struct 1998;43(1):57–70.
[20] Di Sciuva M. An improved shear-deformation theory for moderately thick multilayered anisotropic shells and plates. J Appl Mech 1987;54:589–96.
[21] Cho M, Parmerter RR. An efficient higher-order plate theory for laminated composites. Compos Struct 1992;20(2):113–23.
[22] Zhen W, Wanji C. A global-local higher order theory for multilayered shells and the analysis of laminated cylindrical shell panels. Compos Struct 2008;84(4):350–61.
[23] Batra RC, Vidoli S. Higher-order piezoelectric plate theory derived from a three-dimensional variational principle. AIAA J 2002;40(1):91–104.
[24] Vidoli S, Batra RC. Derivation of plate and rod equations for a piezoelectric body from a mixed three-dimensional variational principle. J Elast 2000;59(1):23–50.
[25] Demasi L. Refined multilayered plate elements based on Murakami zig–zag functions. Compos Struct 2005;70(3):308–16.
[26] Carrera E. Theories and finite elements for multilayered, anisotropic, composite plates and shells. Arch Comput Meth Eng 2002;9(2):87–140.
[27] Vel SS, Batra RC. The generalized plane strain deformations of thick anisotropic composite laminated plates. Int J Solids Struct 2000;37(5):715–33.
[28] Batra RC, Vel SS. Closure to The generalized plane strain deformations of thick anisotropic composite laminated plates. Int J Solids Struct (UK) 2001;38(3):483–9.
[29] Vel SS, Batra RC. Analytical solution for rectangular thick laminated plates subjected to arbitrary boundary conditions. AIAA J 1999;37(11):1464–73.
[30] Reddy JN. Mechanics of laminated composite plates and shells: theory and analysis. CRC; 2004.
[31] Dvorkin EN, Bathe KJ. A continuum mechanics based four-node shell element for general nonlinear analysis. Eng Comput 1984;1(1):77–88.
[32] Arciniega RA, Reddy JN. Tensor-based finite element formulation for geometrically nonlinear analysis of shell structures. Comput Meth Appl Mech Eng 2007;196(4–6):1048–73.
[33] Batra RC, Liang XQ. Finite dynamic deformations of smart structures. Comput Mech 1997;20(5):427–38.
[34] Saada AS. Elasticity: theory and applications. Malabar,FL: Krieger; 1993.
[35] Lo KH, Christensen RM, Wu EM. A high-order theory of plate deformation—part 1: homogeneous plates. J Appl Mech 1977;44:663.
[36] Cho M, Kim KO, Kim MH. Efficient higher-order shell theory for laminated composites. Compos Struct 1996;34(2):197–212.
[37] Batra RC. Elements of continuum mechanics. AIAA; 2006.
[38] Qian LF, Batra RC. Three-dimensional transient heat conduction in a functionally graded thick plate with a higher-order plate theory and a meshless local Petrov–Galerkin method. Comput Mech 2005;35(3):214–26.
[39] Xiao JR, Gilhooley DF, Batra RC, Gillespie JW, Mccarthy MA. Analysis of thick composite laminates using a higher-order shear and normal deformable plate theory (HOSNDPT) and a meshless method. Compos Part B: Eng 2008;39(2):414–27.
[40] Pagano NJ. Exact solutions for composite laminates in cylindrical bending. J Compos Mater 1969;3(3):398–411.
[41] Ren JG. Exact solutions for laminated cylindrical shells in cylindrical bending. Compos Sci Technol 1987;29(3):169–87.
[42] Icardi U, Ruotolo R. Laminated shell model with second-order expansion of the reciprocals of Lamé coefficients H_α, H_β and interlayer continuities fulfilment. Compos Struct 2002;56(3):293–313.
[43] Xavier PB, Lee KH, Chew CH. An improved zig–zag model for the bending of laminated composite shells. Compos Struct 1993;26(3):123–38.
[44] Qian LF, Batra RC, Chen LM. Elastostatic deformations of a thick plate by using a higher-order shear and normal deformable plate theory and two meshless local petrov-galerkin (MLPG) methods. Comput Model Eng Sci 2003;4:161–76.
[45] Qian LF, Batra RC, Chen LM. Free and forced vibrations of thick rectangular plates by using higher-order shear and normal deformable plate theory and meshless petrov-galerkin (MLPG) method. Comput Model Eng Sci 2003;4:519–34.
[46] Qian LF, Batra RC, Chen LM. Static and dynamic deformations of thick functionally graded elastic plate by using higher-order shear and normal deformable plate theory and meshless local petrov-galerkin method. Compos Part B 2004;35:685–97.
[47] Qian LF, Batra RC, Chen LM. Analysis of cylindrical bending thermoelastic deformations of functionally graded plates by a meshless local petrov-galerkin method. Comput Mech 2004;33:263–73.
[48] Qian LF, Batra RC. Design of bidirectional functionally graded plate for optimal natural frequencies. J Sound Vib 2005;280:415–24.
[49] Qian LF, Batra RC. Transient thermoelastic deformations of a thick functionally graded plate. J Therm Stressess 2004;27:705–40.
[50] Gilhooley DF, Batra RC, Xiao JR, McCarthy MA, Gillespie Jr JW. Analysis of thick functionally graded plates by using higher-order shear and normal deformable

plate theory and (MLPG) method with radial basis functions. Compos Struct 2007;80:539–52.
[51] Xiao JR, Batra RC, Gilhooley DF, Gillespie Jr JW, McCarthy MA. Analysis of thick plates by using a higher-order shear and normal deformable plate theory and (MLPG) method with radial basis functions. Comput Meth Appl Mech Eng 2007;196:979–87.
[52] Gilhooley DF, Xiao JR, Batra RC, McCarthy MA, Gillespie Jr JW. Two-dimensional stress analysis of functionally graded solids using the (MLPG) method with radial basis functions. Comput Mater Sci 2008;41:467–81.
[53] Batra RC, Aimmanee S. Vibrations of thick isotropic plates with higher order shear and normal deformable plate theories. Comput Struct 2005;83:934–55.